NACA

RESEARCH MEMORANDUM

INVESTIGATION OF HIGH-SUBSONIC PERFORMANCE CHARACTERISTICS OF A 12° 21-INCH CONICAL DIFFUSER, INCLUDING THE EFFECTS OF CHANGE IN INLET-BOUNDARY-LAYER THICKNESS

By Martin R. Copp and Paul L. Klevatt

Langley Aeronautical Laboratory
Langley Air Force Base, Va.

NATIONAL ADVISORY COMMITTEE FOR AERONAUTICS

WASHINGTON

March 24, 1950

 [redacted]

NATIONAL ADVISORY COMMITTEE FOR AERONAUTICS

RESEARCH MEMORANDUM

INVESTIGATION OF HIGH-SUBSONIC PERFORMANCE CHARACTERISTICS OF A 12° 21-INCH CONICAL DIFFUSER, INCLUDING THE EFFECTS OF CHANGE IN INLET-BOUNDARY-LAYER THICKNESS

By Martin R. Copp and Paul L. Klevatt

SUMMARY

Investigations were conducted of a 12° 21-inch conical diffuser of 2:1 area ratio to determine the interrelation of boundary-layer growth and performance characteristics. Total-pressure and static-pressure surveys were made of inlet and exit flows, longitudinal static pressures were recorded, and velocity profiles were obtained through an inlet Reynolds number range, determined from mass flows and based on inlet diameter of 1.45×10^6 to 7.45×10^6 and a Mach number range of 0.11 to approximately choking. These investigations were made for two thicknesses of inlet boundary layer. The mean value, over the entire range of inlet velocities, of the displacement thickness of the thinner inlet boundary layer was approximately 0.035 inch and that of the thicker inlet boundary layer was approximately six times this value.

The loss coefficient in the case of the thinner inlet boundary layer had a value between 2 to 3 percent of the inlet impact pressure over most of the air-flow range. The loss coefficient with the thicker inlet boundary layer was of the order of twice that of the thinner inlet boundary layer at low speeds and approximately three times at high speeds. In both cases the values were substantially less than those given in the literature for fully developed pipe flow.

The static-pressure rise for the thinner inlet boundary layer was of the order of 95 percent of that theoretically possible over the entire speed range. For the thicker inlet boundary layer the static-pressure rise, as a percentage of that theoretically possible, ranged from 82 percent at low speeds to 68 percent at high speeds.

[redacted]

INTRODUCTION

Low efficiencies and high pressure losses in the intake systems of jet power plants have been attributed by many investigators to the separation of the boundary layer from the duct walls. At the present time, there are few data available on the relationships between separation, boundary-layer thickness and shape characteristics, and diffuser performance, particularly in the high Reynolds number and high-subsonic Mach number range. The present investigation presents basic data needed to give a better understanding of the mechanism of losses in diffusers. References 1 to 6 summarize a large portion of the existing data on subsonic diffuser performance. In certain cases, the inlet-boundary-layer conditions were varied. Some investigations were conducted with air-flow rates approaching choking quantities, but small inlet diameters prevented the Reynolds numbers from reaching the range encountered in flight. Other diffusers, the sizes of which were comparable to those used in present-day aircraft, were tested, but power limitations prevented both Mach and Reynolds numbers from approaching the values reached by high-subsonic-speed aircraft. The present investigation was initiated as part of a program to determine the interrelation of boundary-layer growth and performance characteristics in full-scale internal-flow systems at inlet Reynolds and Mach numbers characteristic of those encountered in flight.

The data presented hereinafter were obtained from investigations conducted in the Langley induction aerodynamics laboratory of a 12° conical diffuser with two different inlet-boundary-layer conditions, through an inlet Reynolds number range determined from mass flows and based on inlet diameter of 1.45×10^6 to 7.45×10^6 and an inlet Mach number range of 0.11 to approximately choking. Thickening of the inlet boundary layer was accomplished by the addition of a straight pipe to the diffuser inlet. Over-all performance characteristics, including longitudinal static-pressure distributions, as well as velocity profiles and values of boundary-layer-shape parameters, are presented. Conical diffusers having other inlet diameters and diffusion angles are now in the process of being investigated as a continuation of the program.

SYMBOLS

p	static pressure
H	total pressure
H_o	reference total pressure

M_1	one-dimensional theoretical Mach number corresponding to the pressure ratio p_i/H_o
w	weight flow
T_o	total temperature, degrees F
ΔH	weighted total-pressure loss from mass-flow surveys $(H_i - H_e)$
Δp	static-pressure rise measured at wall $(p_e - p_i)$
q_c	impact pressure $(H - p)$
Δq_c	change in impact pressure $(q_{ci} - q_{ce})$
u	local velocity within the boundary layer
U	local velocity at the edge of the boundary layer
x	longitudinal distance along diffuser center line
u/U	velocity ratio for incompressible flow $\left(\sqrt{\frac{H - p_{wall}}{H_{max} - p_{wall}}}\right)$
δ	boundary-layer thickness at 0.95u/U
δ^*	boundary-layer displacement thickness for incompressible flow $\int_0^{\delta'} \left(1 - \frac{u}{U}\right)dy$
θ	boundary-layer momentum thickness for incompressible flow $\int_0^{\delta'} \frac{u}{U}\left(1 - \frac{u}{U}\right)dy$
δ'	distance from surface beyond which the contribution to the integrals of δ^* and θ is negligible
δ^*/θ	boundary-layer-shape parameter for incompressible flow
$\Delta H/q_{ci}$	loss coefficient
$\Delta p/\Delta q_c$	pressure efficiency
$\Delta q_c/\Delta q_{c_{ideal}}$	diffusion factor

$\Delta p/\Delta p_{ideal}$ diffuser effectiveness

Subscripts:

i diffuser inlet conditions measured at duct wall

e diffuser exit conditions measured at duct wall

1,2,3,4,5,6 boundary-layer stations

APPARATUS AND TESTS

A line drawing of the test apparatus is shown in figure 1. This apparatus is preceded by a plenum chamber of 4900-cubic-foot capacity into which a maximum of 130,000 cubic feet of air per minute at a pressure rise of 58 inches of water is discharged from three 1000-horsepower centrifugal compressors. From the plenum chamber, the air passes through a 16-mesh wire screen with a free area ratio of 0.552 and into an entrance bell with a contraction ratio of 6.6:1 designed to give a uniform velocity over the diffuser inlet.

The diffuser has a total expansion angle of 12°, an inlet diameter of 21 inches, and an area ratio of 2:1. A cylindrical tail pipe 75 inches long follows the diffuser. Thickening of the boundary layer is accomplished by the insertion of a straight pipe 89 inches long between the bell and diffuser inlet. The bell, inlet section, diffuser, and tail pipe are all of 16-gage duralumin construction. In order to insure surface smoothness, all joints were sealed with a pyroxylin compound, painted, and sanded. Photographs of the two configurations with instrumentation in place are shown in figures 2 and 3.

Six equally spaced, 0.040-inch static-pressure orifices were installed flush with the wall around the inlet periphery and another set of six at the exit section. A third series was placed along the generatrix of the diffuser to record longitudinal pressure distributions. Similar static orifices lined the transition section joining the inlet length to the diffuser, as shown in figure 1. All static-pressure orifices were connected to a multitube manometer and pressures recorded photographically.

Mass-flow surveys at approximately 1-inch intervals were made across the stream at the diffuser inlet and exit sections by two remotely controlled, electrically driven, pitot-static tubes placed 120° apart. A perspective drawing of the type of tube used is shown in figure 1. After surveying the exit section at the desired mass flows, the tubes were placed in the inlet section and surveys were repeated at corresponding mass flows. Figures 1, 2, and 3 indicate the positions of the mass-flow survey tubes for inlet and exit surveys. Reference total pressure referred to atmospheric pressure was measured by a total-pressure tube placed upstream of the entrance bell. Total temperatures were measured by a shielded iron-constantan thermocouple connected to a sensitive potentiometer. The thermocouple was placed diametrically opposite the stagnation-pressure tube, as shown in figure 1.

Total-pressure surveys across the boundary layer were made at six stations along the diffuser (fig. 1) by using a remotely controlled impact tube with an outside diameter of 0.050 inch and a wall thickness of 0.010 inch. The end of the tube was flattened and filed to an oval-shape opening 0.003 inch high and 0.060 inch wide, as seen in figure 1. Wall static pressures were recorded simultaneously with each total-pressure reading. Curves of inlet-flow characteristics, including M_i, Reynolds number, and weight flow against p_i/H_o, are given in figures 4(a) and 4(b). The curve of Reynolds number, based on inlet diameter, is included for general interest; but it should be borne in mind that the thickness of the boundary layer, rather than the duct diameter, is of more significance in determining the Reynolds number effect. The coordinates of figure 4(b) were chosen as a convenient method of representing the relation of mass flow to p_i/H_o. For standard stagnation conditions of 29.92 inches of mercury and 60° F, this curve gives the weight flow directly in pounds per second as a function of the pressure ratio p_i/H_o.

METHODS OF ANALYSIS

Computation methods.- Total-pressure and static-pressure measurements at the diffuser entrance and exit, as well as longitudinal static pressures, were made over the complete range of inlet velocities investigated. All pressures were referred to the reference total pressure measured upstream of the inlet bell. The total-pressure losses through the diffuser were determined from a mass-flow weighted average of the pitot-static traverses taken at the diffuser entrance and exit. The total-pressure loss was obtained from the relation:

$$\frac{\Delta H}{H_o} = \frac{\overline{H_o - H_e}}{H_o} - \frac{\overline{H_o - H_i}}{H_o}$$

The impact-pressure change through the diffuser was calculated from the following expression:

$$\frac{\Delta q_c}{H_o} = \frac{q_{ci}}{H_o} - \frac{q_{ce}}{H_o}$$

or

$$\frac{\Delta q_c}{H_o} = \left(\frac{H_o - p_i}{H_o} - \frac{\overline{H_o - H_i}}{H_o}\right) - \left(\frac{H_o - p_e}{H_o} - \frac{\overline{H_o - H_e}}{H_o}\right)$$

Performance parameters.- Since diffusers are utilized under varying conditions and for numerous purposes, certain performance parameters are sometimes of greater interest than others. It is frequently desirable to consider the loss of total pressure incurred by a diffuser quite separately from its performance in increasing static pressure. The loss coefficient $\Delta H/q_{ci}$ is a satisfactory index of the loss characteristics of a diffuser. This parameter possesses the advantage of tending to be constant over a range of flow rates and density, unless changes in these variables are accompanied by changes in flow pattern.

The static-pressure rise effected by a diffuser is a consequence of two interconnected actions. As the stream area is increased, impact pressure is converted to other forms of energy. Of the impact pressure converted, only part appears as developed static pressure in the diffuser exit, the remainder $\left(\text{that part measured by the loss coefficient } \frac{\Delta H}{q_{ci}}\right)$ being expended in overcoming friction and turbulence losses within the diffuser. The efficiency of conversion of impact pressure to useful static pressure is measured by the ratio:

$$\frac{\Delta p_{actual}}{\Delta q_{c_{actual}}}$$

which will be referred to as pressure efficiency.

Regardless of the efficiency of the diffuser in other respects, if, for such reasons as thickening of the boundary layer, that part of the stream bearing most of the kinetic energy undergoes less proportional area increase than does the diffuser, the conversion of impact pressure will be less than theoretically possible and the obtainable static-pressure increase is thereby limited. The conversion of the available impact pressure is measured by the ratio:

$$\frac{\Delta q_{c_{actual}}}{\Delta q_{c_{ideal}}}$$

and will be referred to as diffusion factor.

The ideal reduction in impact pressure, which is identical with the ideal rise in static pressure, is that which would occur for the area ratio under consideration if the flow were uniform and isentropic.

The ratio of actual pressure rise $\left(\Delta p_{actual}\right)$ to that theoretically possible $\left(\Delta p_{ideal} = \Delta q_{c_{ideal}}\right)$ which is the most convenient over-all measure of the pressure-producing abilities of a diffuser, termed the diffuser effectiveness, is the product of the pressure efficiency and the diffusion factor. Therefore,

$$\frac{\Delta p_{actual}}{\Delta q_{c_{actual}}} \frac{\Delta q_{c_{actual}}}{\Delta q_{c_{ideal}}} = \frac{\Delta p_{actual}}{\Delta q_{c_{ideal}}} = \frac{\Delta p_{actual}}{\Delta p_{ideal}}$$

RESULTS AND DISCUSSION

Pressure-Survey Results

Loss coefficient $(\Delta H/q_{ci})$.- The performance of the two configurations investigated, in terms of the loss coefficient $\Delta H/q_{ci}$ against the ratio of the inlet static to upstream total pressure p_i/H_o, is shown in figure 5. The parameter p_i/H_o was chosen as an approximate index of inlet Mach number. Movement to the right on the curve is in the order of increasing Mach number and air-flow rate. No attempt was made to isolate Mach number and Reynolds number effects. For the thinner inlet boundary layer, the loss coefficient is fairly constant at a value of approximately 0.024 until a p_i/H_o of about 0.68 is reached; this constancy indicates that the flow pattern has remained essentially unchanged. After this point, the loss coefficient rises steadily to a p_i/H_o of approximately 0.59, where it breaks sharply into the region of higher losses due to the attainment of local sonic velocities at the wall (see figs. 5 and 9). The loss coefficient for the thicker inlet boundary layer shows a steady rise over the complete range of inlet velocities investigated, which is indicative of a constantly changing flow pattern due to the influence of the thickened inlet boundary layer.

For fully developed pipe flow, for which the displacement thickness for this sized inlet would be about 1 inch, the loss coefficient from the literature (reference 5) is 0.055. In comparing this value with data from the current test it should be borne in mind that the reference data are for a Reynolds number, based on pipe diameter, of 120,000 and the lowest values in the current tests are of the order of 1,500,000.

In either configuration any attempt to increase the flow rate beyond the choking value inevitably results in large shock losses. Where the choking value of the diffuser mass flow is insufficient for the needs of a particular application, the onset of high losses can be delayed by enlargement of the inlet diameter. It is apparent that for equal mass flows at the point of onset of large losses a slightly larger inlet diameter would be needed for the thicker inlet boundary layer than that used for the thinner inlet boundary layer.

Pressure efficiency $(\Delta p/\Delta q_c)$.- The pressure efficiency for the thinner inlet boundary layer, as shown in figure 6, remains essentially constant at values close to 97 percent, tapering off to approximately 86 percent at the highest inlet velocities where local sonic velocity is attained on the duct walls. The pressure efficiency for the thicker inlet boundary layer remains over 90 percent for most of the inlet velocities, gradually decreasing to approximately 87 percent as sonic velocity is approached. The absence of a sharp decrease in pressure efficiency reflects the absence of any sharp increase in the loss coefficient.

Diffusion factor $\left(\Delta q_c/\Delta q_{c_{ideal}}\right)$.- Figure 7 indicates constantly high values for the thinner inlet boundary-layer case which can be attributed to the fact that the rate of increase of cross-sectional area of the high-velocity stream is essentially that of the duct. A sharp decrease in diffusion factor suggests the appearance of flow breakdown or a sudden increase in boundary-layer thickness in the critical-flow range. The most outstanding effect of thickening the inlet boundary layer is the substantial reduction in diffusion factor shown by the lower curve of figure 7.

Diffuser effectiveness $\left(\Delta p/\Delta p_{ideal}\right)$.- Although the pressure efficiency was less with the thicker boundary layer, the effect was relatively small and the reduction in diffusion factor was the dominant cause for the reduction in diffuser effectiveness (fig. 8) which resulted from a thicker inlet boundary layer.

Static-pressure distribution.- The diffuser performance, as well as the boundary-layer growth and flow separation, is dependent not only upon inlet conditions but also upon the longitudinal static-pressure gradients. Figures 9 to 11 show the static-pressure distribution for the two configurations as a function of the pressure ratio p/H_o and the distance along the diffuser axis for several representative inlet velocities. The distributions show a velocity increase around the transition section which can be attributed to the effects of local wall curvature. The lowest values of p/H_o for the representative inlet velocities shown in figures 9 to 11 occur slightly downstream of the half length of arc of the transition section. Similar results were observed in the work of reference 7. Local sonic velocities first occurred on the diffuser wall at an entrance Mach number of about 0.89 for the thinner inlet boundary layer and 0.93 for the thicker inlet boundary layer. A comparison of pressure distributions at similar entrance Mach numbers for both configurations is shown in figure 11. It appears that the thicker inlet boundary layer reduces both the acceleration around the transition section and the static-pressure recovery through the diffuser, as shown in figure 8. In interpreting the static-pressure curves, it should be borne in mind that the ordinate values of p/H_o are not precise measures of the Mach number across the diffuser inasmuch as the region of flow around a curvature produces gradients which are transverse to the stream so that minimum pressures measured at the walls must necessarily be less than at a point in midstream.

Boundary-Layer Results

Thinner inlet boundary layer.- Velocity profiles and boundary-layer-shape parameters for the thinner-inlet-boundary-layer diffuser are presented in figures 12 to 19. Due to the fact that the majority of existing boundary-layer data is in incompressible form, the quantities δ^*, θ, δ^*/θ, and boundary-layer profiles for this investigation were computed in a similar manner so that a comparison could be effected. All of the velocity profiles in figures 12(a) to 12(e) were obtained from the boundary-layer survey tube shown in figure 3. The data presented with each profile consist of the inlet pressure ratio, the local pressure ratio, and the total temperature. Since the momentum thickness can be obtained from figure 17, the value of R_θ can be computed for any profile. Profiles obtained with the mass-flow survey tubes are presented in figures 13(a) and 13(c). Since they are in the same plane as boundary-layer station 6, although 120° apart, the velocity profile of station 6 (fig. 12(e)) has been reproduced in figure 13(b) for comparison. The velocity profile of figure 13(b) was not obtained simultaneously with those of figures 13(a) and 13(c), which accounts for the difference in the values of p_i/H_o. However, the similarity of profile shapes is apparent.

The velocity profile obtained at station 5 (fig. 12(c)) indicates high velocities occurring close to the duct wall. Although this was the only one of its type observed in these surveys, in other investigations, as yet unpublished, similar profiles have been found to exist simultaneously with separated profiles. This flow condition has been observed at the same station but at different circumferential locations from the separated profiles.

The rate of longitudinal growth of the displacement thickness and momentum thickness of the thinner inlet boundary layer was little affected by changes in inlet velocity at the lowest speeds (figs. 16 and 18). At high inlet velocities, however, a rapid increase in thickness occurs between stations 1 and 2 with correspondingly greater thicknesses at all points downstream.

Thicker inlet boundary layer.– A straight pipe 89 inches long was inserted between the entrance bell and the diffuser to thicken the inlet boundary layer. A complete investigation similar to that conducted with the thinner-inlet-boundary-layer diffuser was made to determine the effects of the thickened boundary layer upon the flow characteristics. The initial boundary layer was thickened about six times that of the thinner-inlet-boundary-layer diffuser. Velocity profiles and boundary-layer-shape parameters for the thicker-inlet-boundary-layer diffuser are presented in figures 20 to 27.

Separation has occurred at station 6 (fig. 20(d)) at a p_i/H_o of 0.552. However, at higher inlet velocities, station 6 (fig. 20(e)), reattachment occurs. Velocity profiles obtained with the mass-flow survey tubes are presented in figures 21(a) and 21(c) and compared with the separated profile (fig. 20(d)) which has been reproduced in figure 21(b). Although the inlet pressure ratios are nearly identical, the profiles differ considerably at the three equidistant positions on the exit circumference of the diffuser. The unstable flow conditions at the diffuser exit, caused by thickening the inlet boundary layer, are reflected in the decreased diffuser performance.

The rate of longitudinal growth of the displacement thickness and momentum thickness of the thicker inlet boundary layer was relatively unaffected by inlet velocity over the entire speed range (figs. 24 and 26).

Due to instrumentation difficulties, it was found impracticable to make boundary-layer surveys at the transition region between the inlet section and the diffuser.

CONCLUSIONS

An investigation was made of the performance characteristics and boundary-layer growth in a 12° 21-inch conical diffuser over an inlet Mach number range of 0.11 to approximately choking and an inlet Reynolds number range from 1.45×10^{6} to 7.45×10^{6}. These investigations were made for two thicknesses of inlet boundary layer. The mean value, over the entire range of inlet velocities, of the displacement thickness of the thinner inlet boundary layer was approximately 0.035 inch and that of the thicker inlet boundary layer was approximately six times this value. For these particular configurations, the following conclusions may be drawn:

1. The static-pressure rise with the thinner inlet boundary layer was approximately 95 percent of the ideal value over most of the inlet-velocity range and decreased abruptly near the onset of choking.

2. When the inlet boundary layer was thickened the maximum static-pressure rise was approximately 82 percent of the ideal value in the low inlet-velocity range. This value decreased steadily until a value of 68 percent was reached at the highest inlet velocity attainable which was just short of the choking condition.

3. The total-pressure loss with the thinner inlet boundary layer, as a fraction of the impact pressure, remained between 2 and 3 percent over most of the range of inlet velocities and rose abruptly when choking conditions were reached.

4. For the case of the thicker inlet boundary layer, the total-pressure loss rose continuously from about 4.3 percent of the inlet impact pressure at the lowest inlet velocity to about 9.5 percent at the highest inlet velocity corresponding to inlet choking conditions. The loss coefficient of the thicker inlet boundary layer was approximately twice that of the thinner inlet boundary layer at low inlet velocities. At velocities approaching the choking condition, however, the loss coefficient was almost three times that of the thinner-inlet-boundary-layer diffuser.

5. The rate of longitudinal growth of the displacement thickness and momentum thickness of the thinner inlet boundary layer was little affected by changes in inlet velocity at the lowest speeds. At high inlet velocities, however, a rapid increase in thickness occurs between stations 1 and 2 with correspondingly greater thicknesses at all points downstream.

6. The rate of longitudinal growth of the displacement thickness and momentum thickness of the thicker inlet boundary layer was relatively unaffected by inlet velocity over the entire speed range.

7. For the thinner inlet boundary layer, no evidence of separation was found at any point in the diffuser over the complete range of inlet velocities. The thicker inlet boundary layer also remained unseparated over most of the inlet velocity range. At inlet velocities near choking, however, separation of the thicker inlet boundary layer was observed to occur near the exit of the diffuser.

Langley Aeronautical Laboratory
National Advisory Committee for Aeronautics
Langley Air Force Base, Va.

REFERENCES

1. Gibson, A. H.: On the Flow of Water through Pipes and Passages Having Converging or Diverging Boundaries. Proc. Roy. Soc. (London), ser. A, vol. 83, no. 563, March 2, 1910, pp. 366–378.

2. Bohm, H., and Koppe, M.: The Influence of Friction on Steady Diffuser Flows at High Speed. Joint Intelligence Objectives Agency (Washington), July 23, 1946.

3. Naumann: Wirkungsgrad von Diffusoren bei hohen Unterschallgeschwindigkeiten. FB Nr. 1705, Deutsche Luftfahrtforschung (Berlin-Adlershof), 1942.

4. Peters, H.: Conversion of Energy in Cross-Sectional Divergences under Different Conditions of Inflow. NACA TM 737, 1934.

5. Henry, John R.: Design of Power-Plant Installations. Pressure-Loss Characteristics of Duct Components. NACA ARR L4F26, 1944.

6. Patterson, G. N.: Modern Diffuser Design. Aircraft Engineering, vol. X, no. 115, Sept. 1938, pp. 267–273.

7. Froessel, W.: Investigation of Compressible Flow on and near a Curved Profile. AAF Translation No. F-TS-1517-RE, Air Materiel Command, Wright Field, Dayton, Ohio, Aug. 1947.

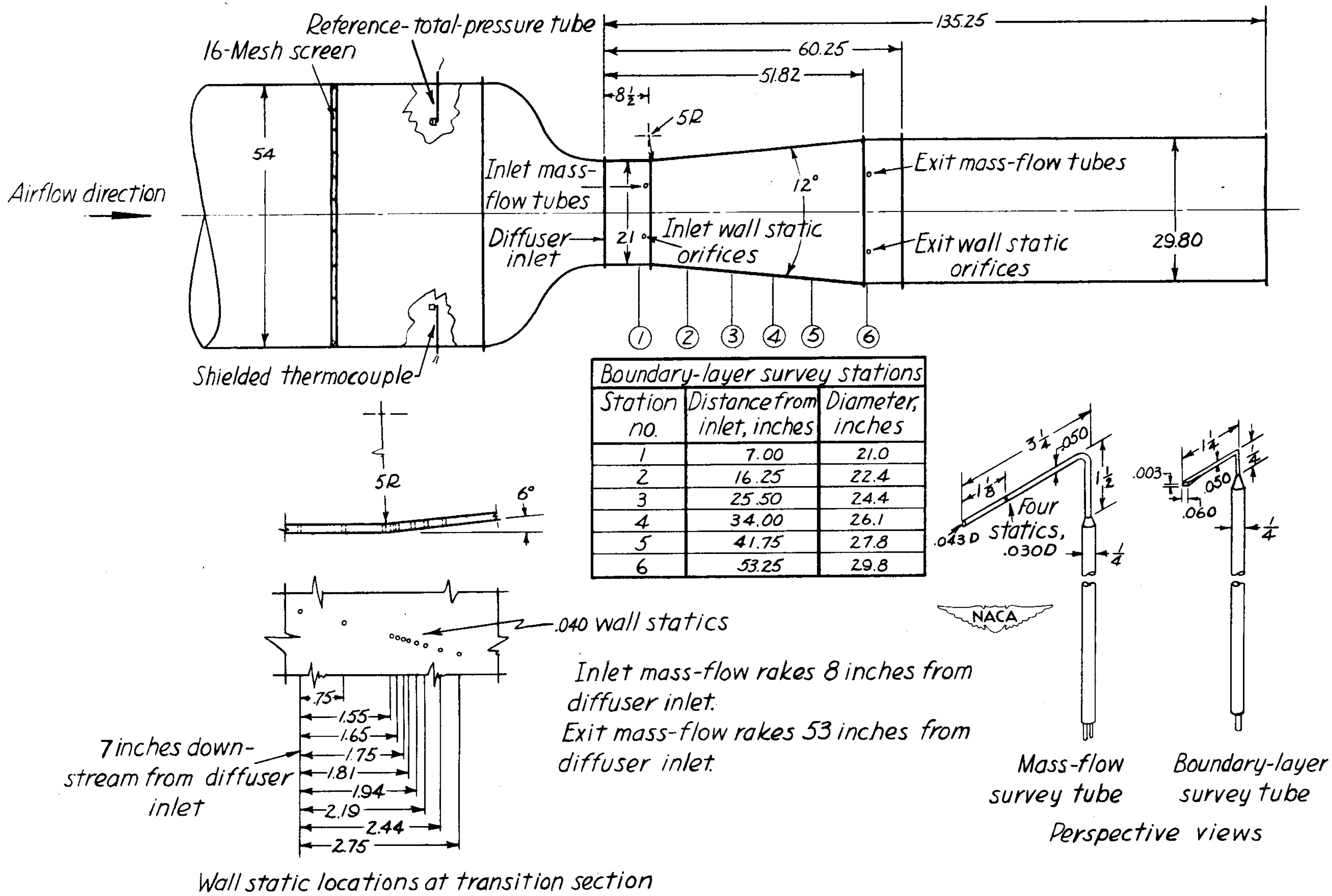

Boundary-layer survey stations

Station no.	Distance from inlet, inches	Diameter, inches
1	7.00	21.0
2	16.25	22.4
3	25.50	24.4
4	34.00	26.1
5	41.75	27.8
6	53.25	29.8

Figure 1.- General arrangement of test setup and instrumentation. All dimensions in inches.

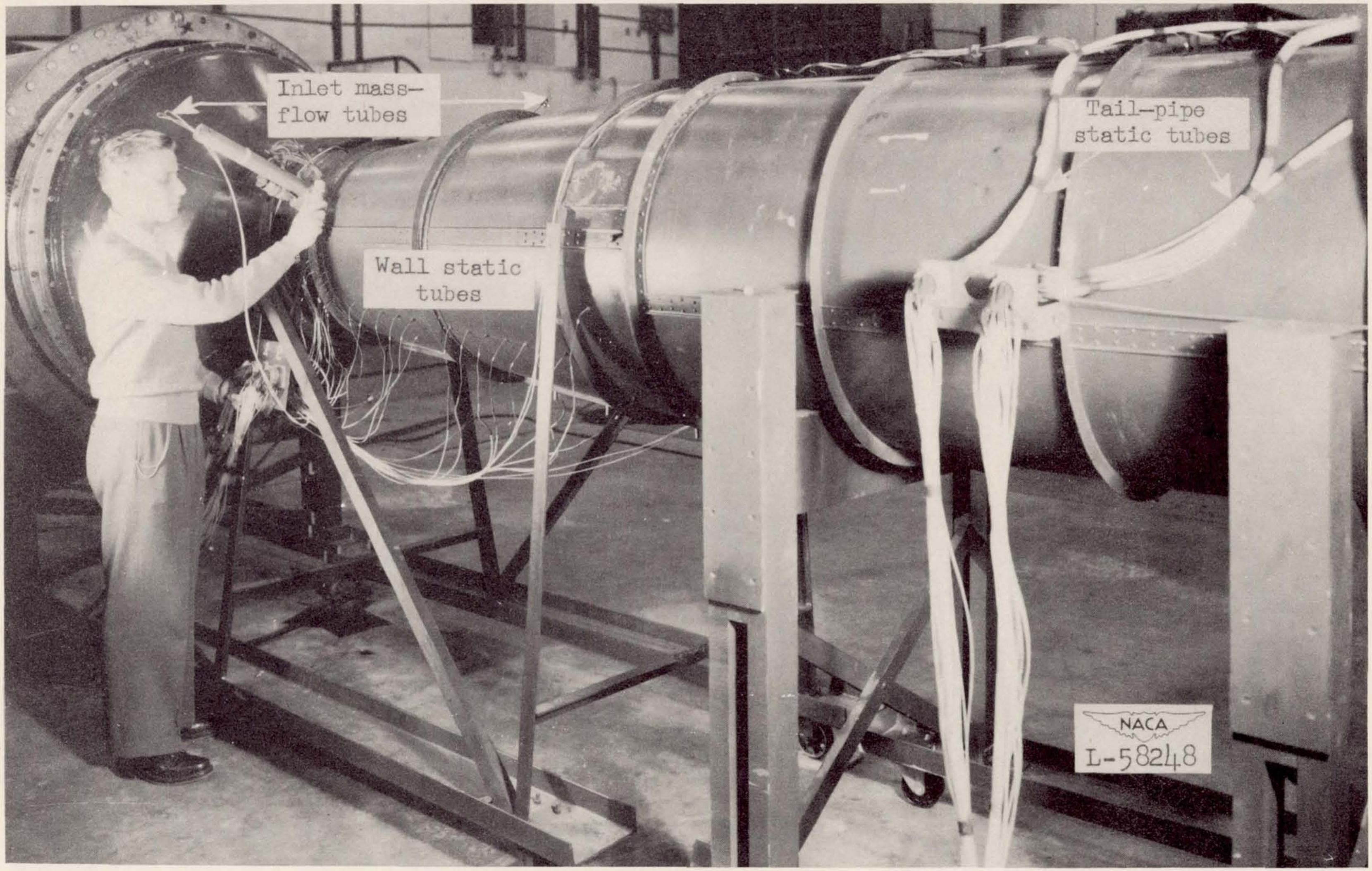

Figure 2.- Test setup for thinner inlet boundary-layer diffuser.

Page intentionally left blank

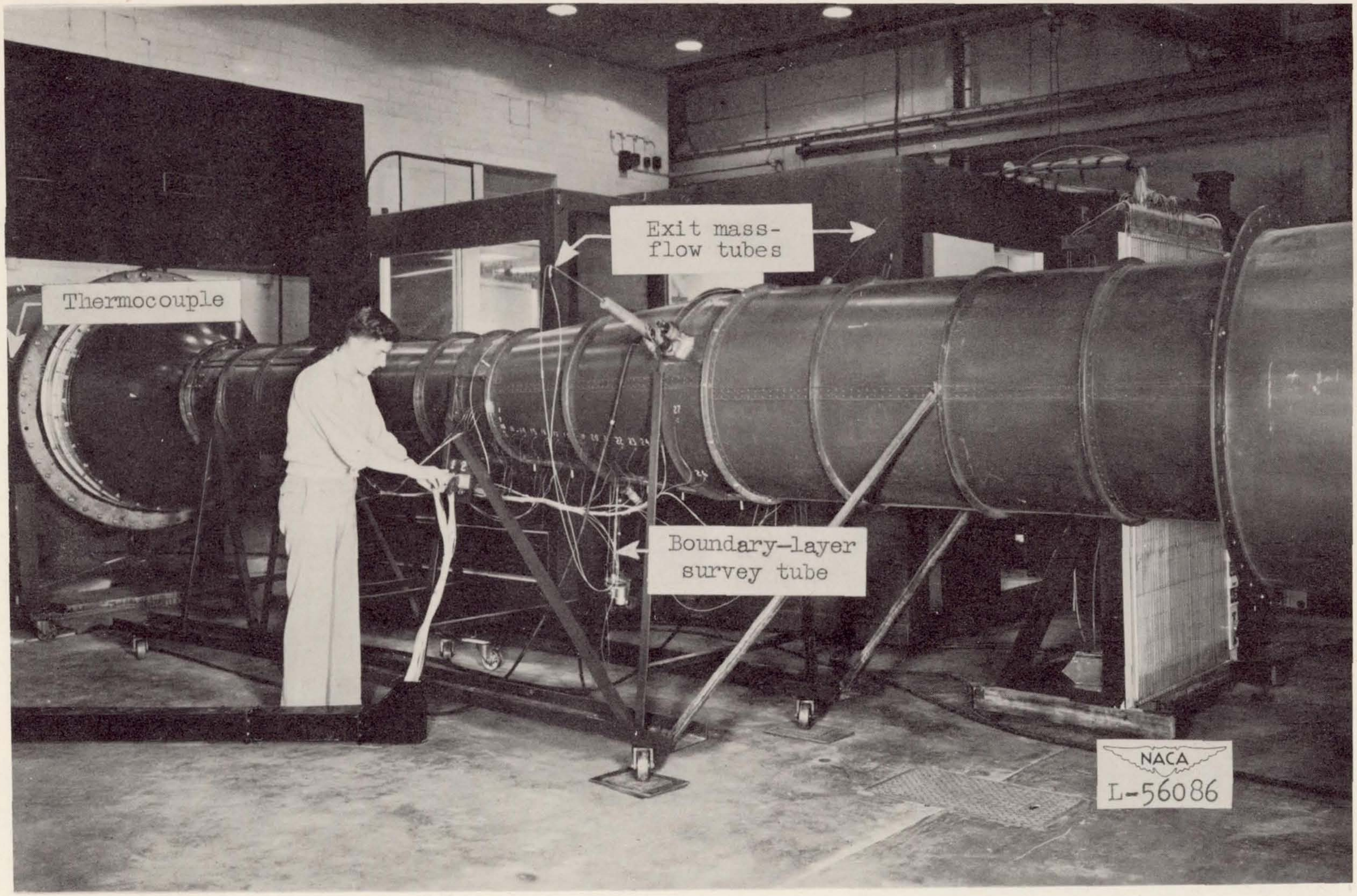

Figure 3.- Test setup for thicker inlet boundary-layer diffuser.

Page intentionally left blank

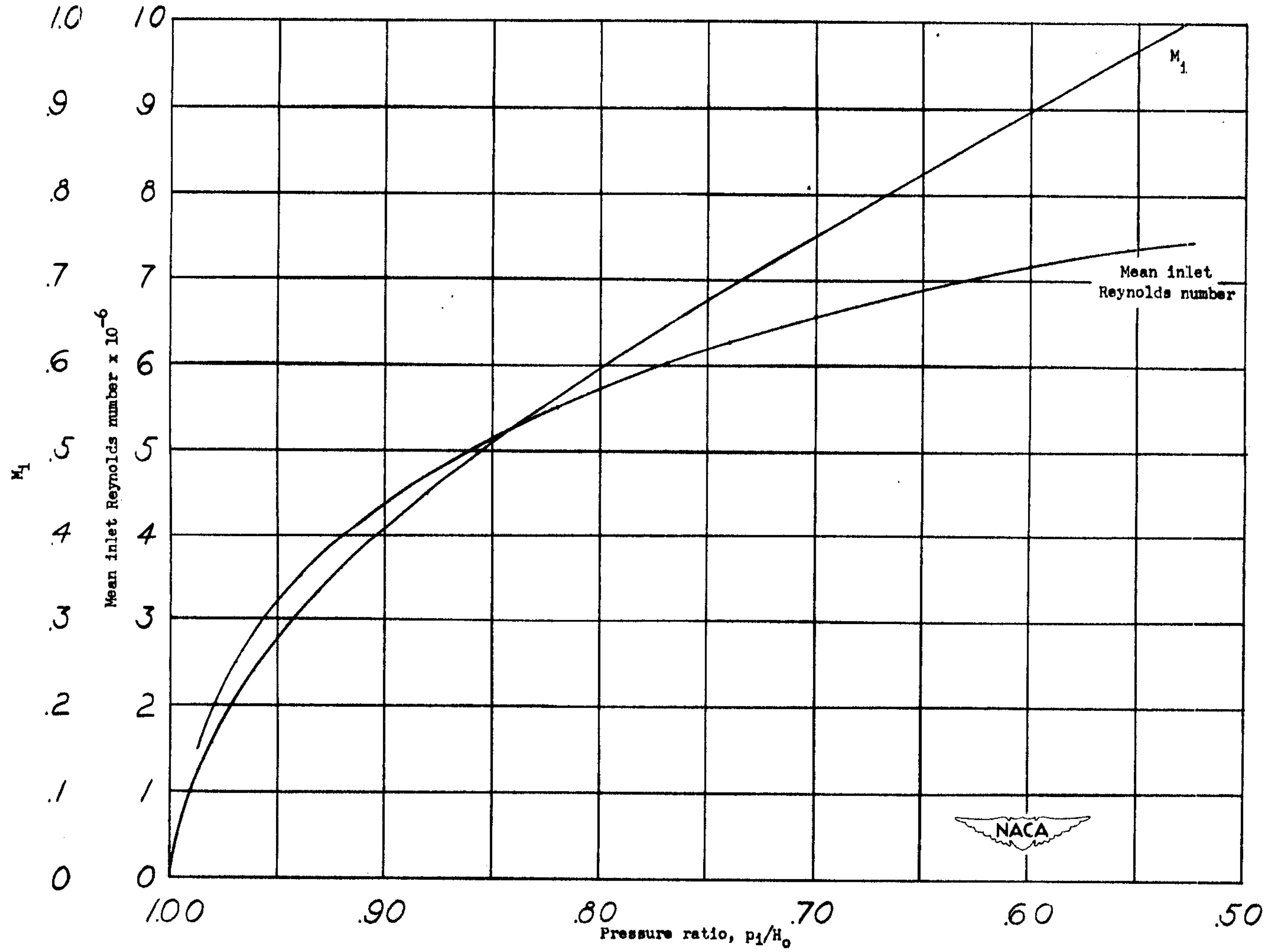

(a) Variation of mean inlet Reynolds number and M_1 with inlet pressure ratio.

Figure 4.- Inlet flow characteristics.

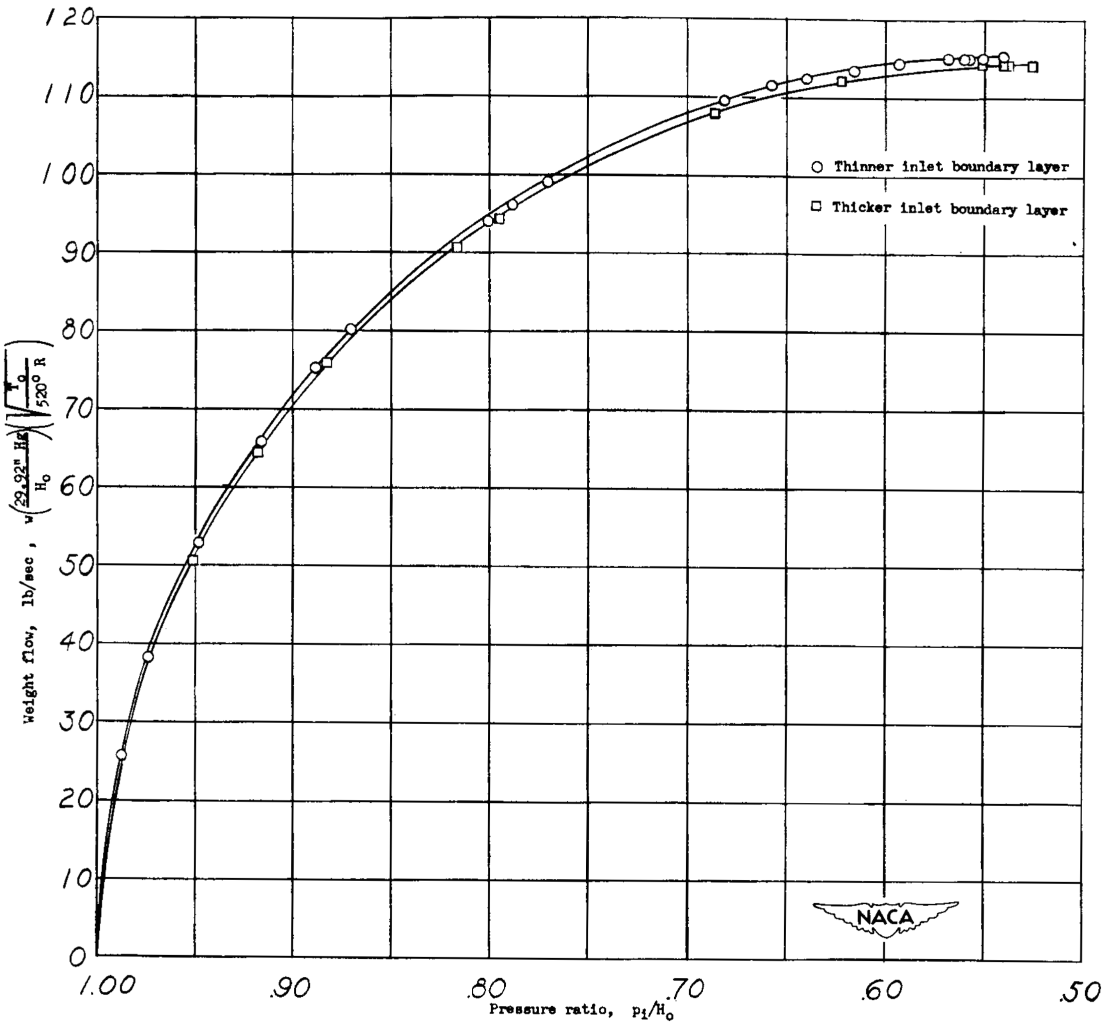

(b) Variation of weight flow with pressure ratio.

Figure 4.- Concluded.

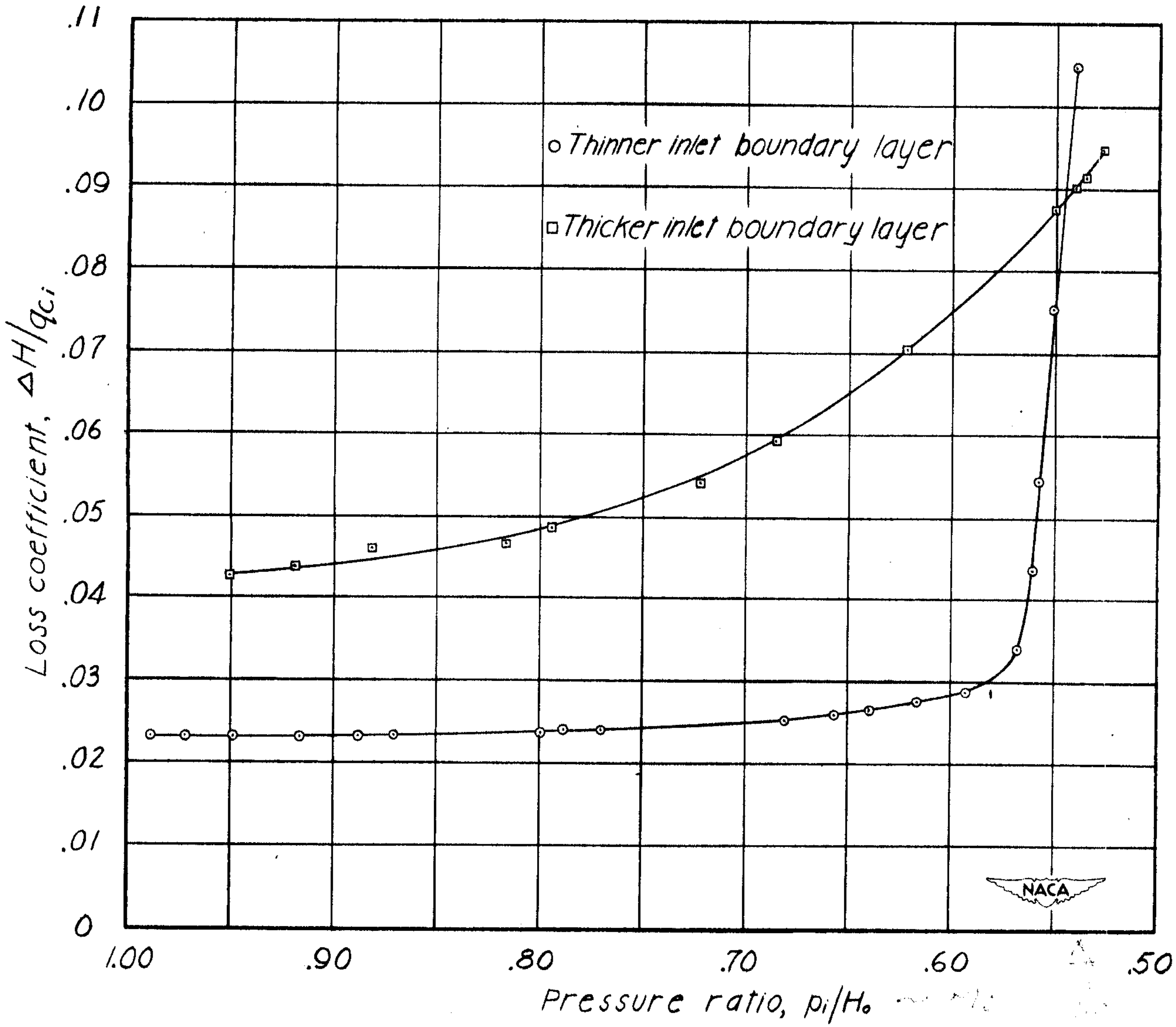

Figure 5.- Variation of loss coefficient with pressure ratio.

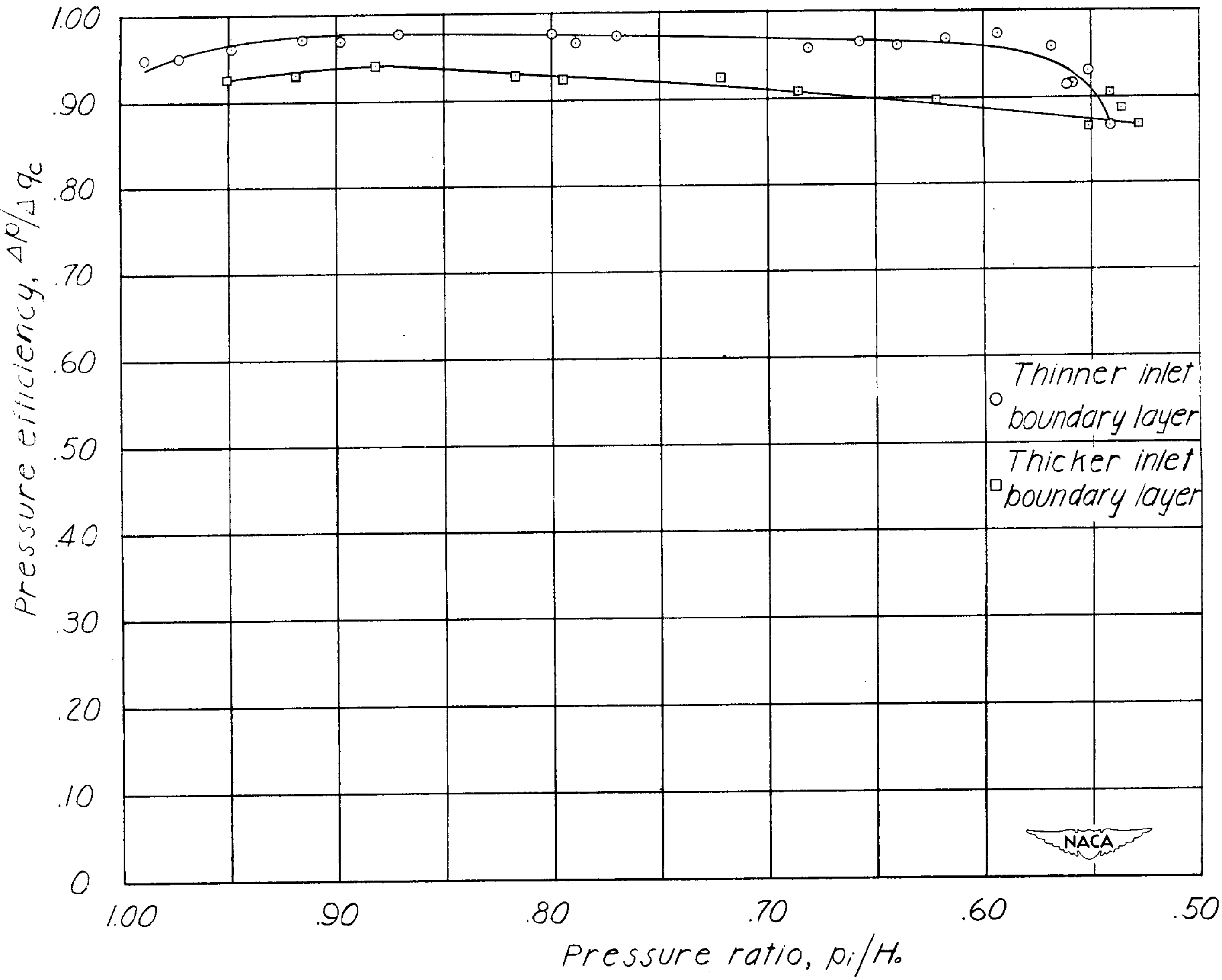

Figure 6.- Variation of pressure efficiency with pressure ratio.

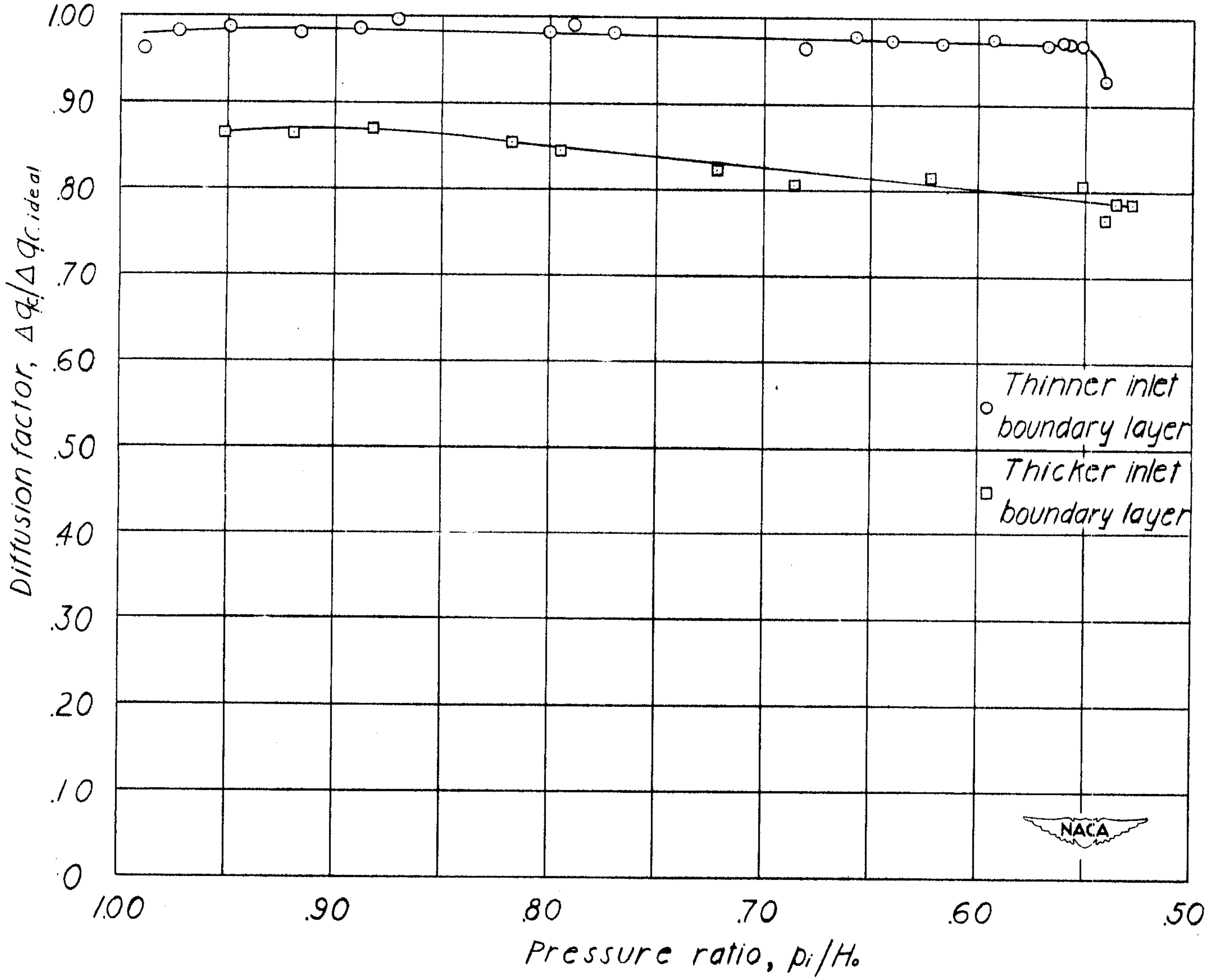

Figure 7.- Variation of diffusion factor with pressure ratio.

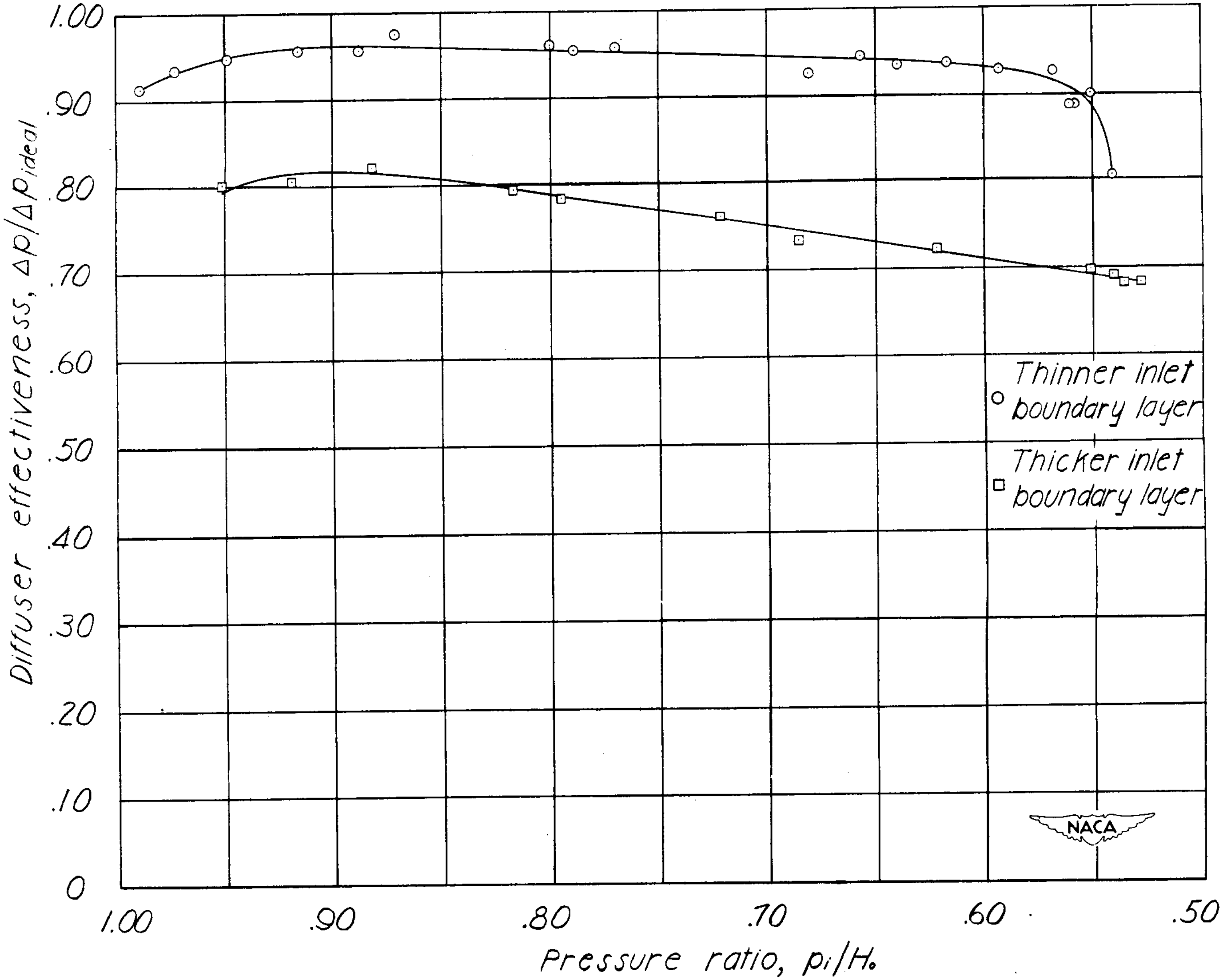

Figure 8.- Variation of diffuser effectiveness with pressure ratio.

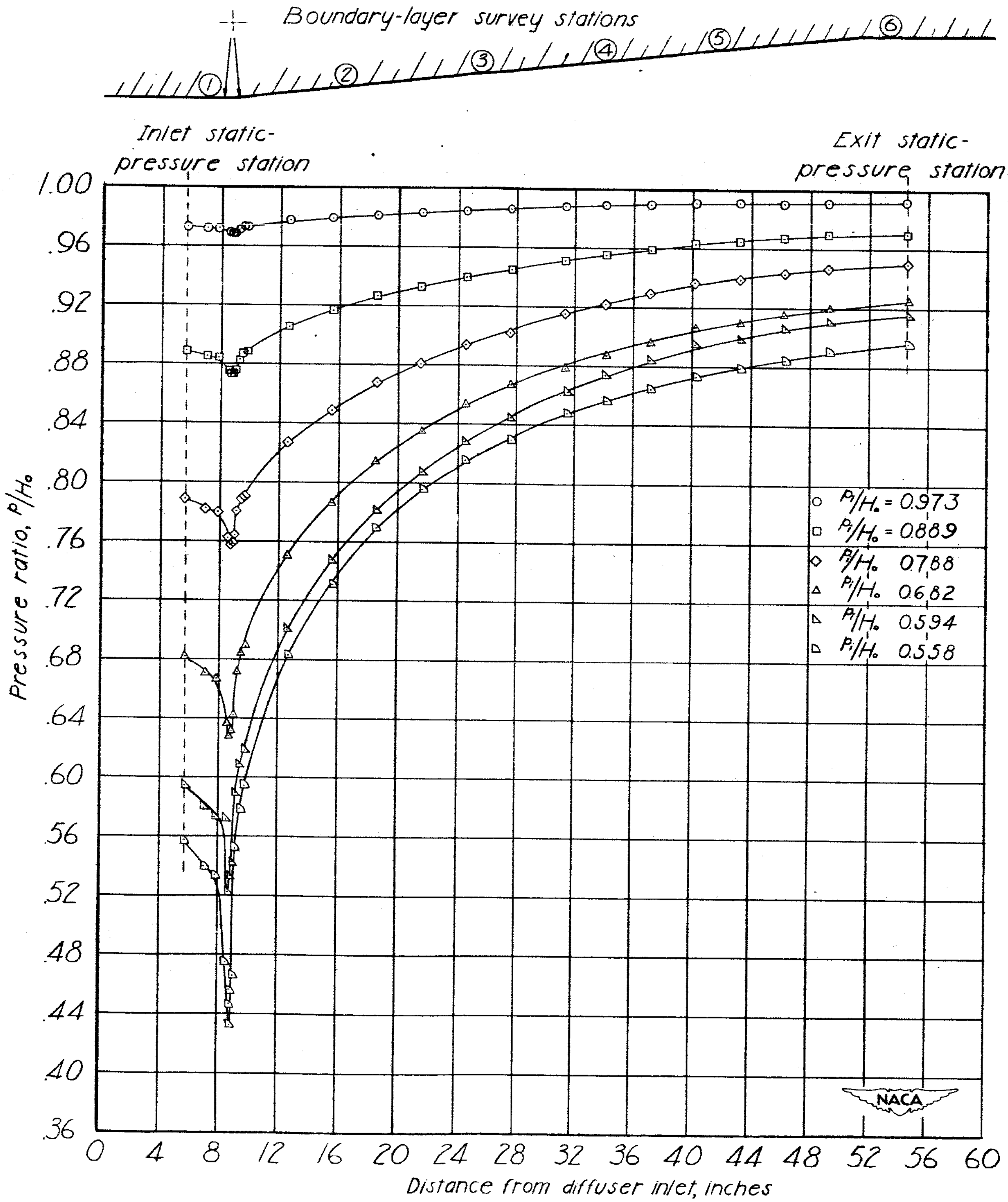

Figure 9.- Static-pressure distribution; thinner inlet boundary layer.

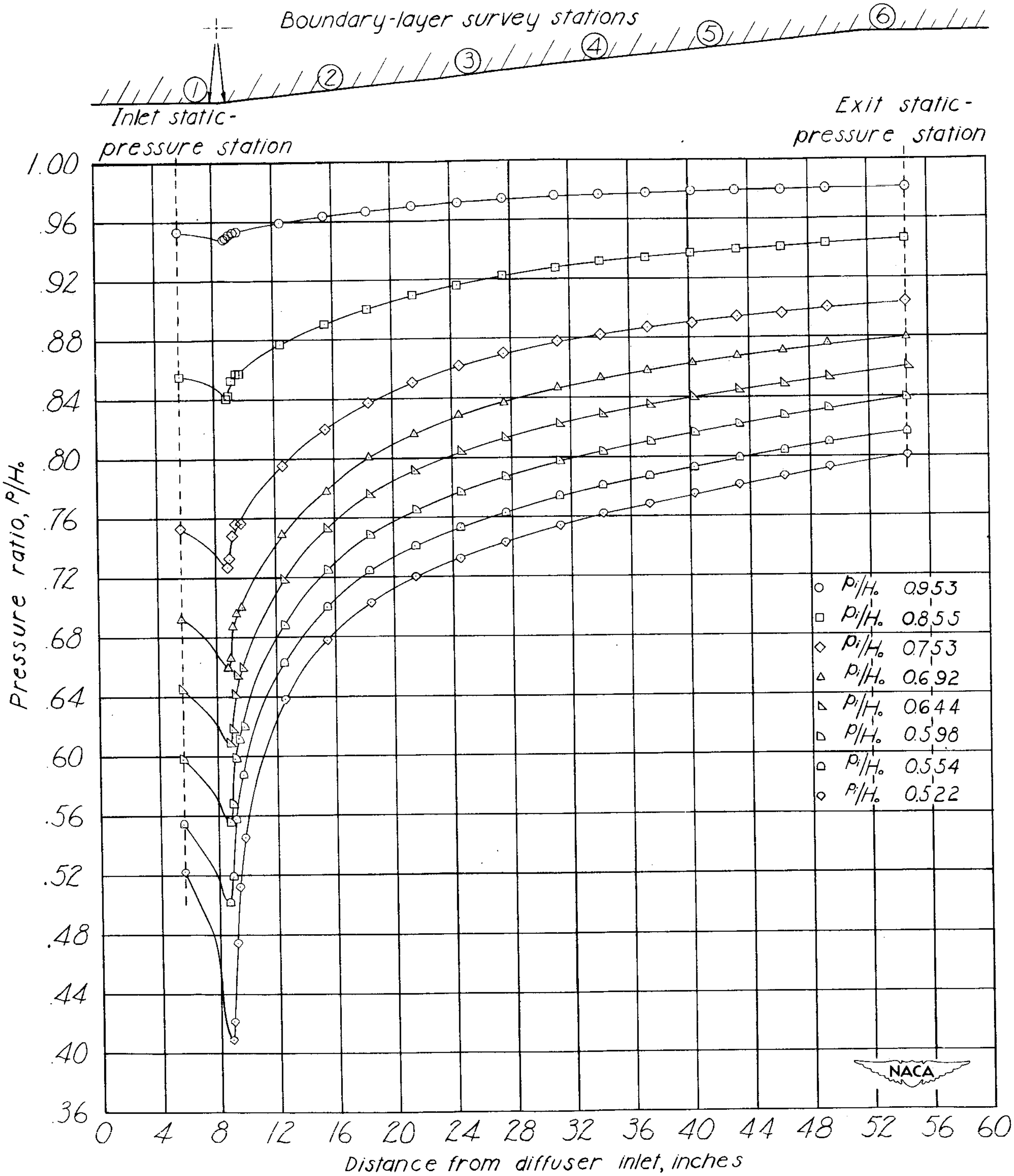

Figure 10.- Static-pressure distribution; thicker inlet boundary layer.

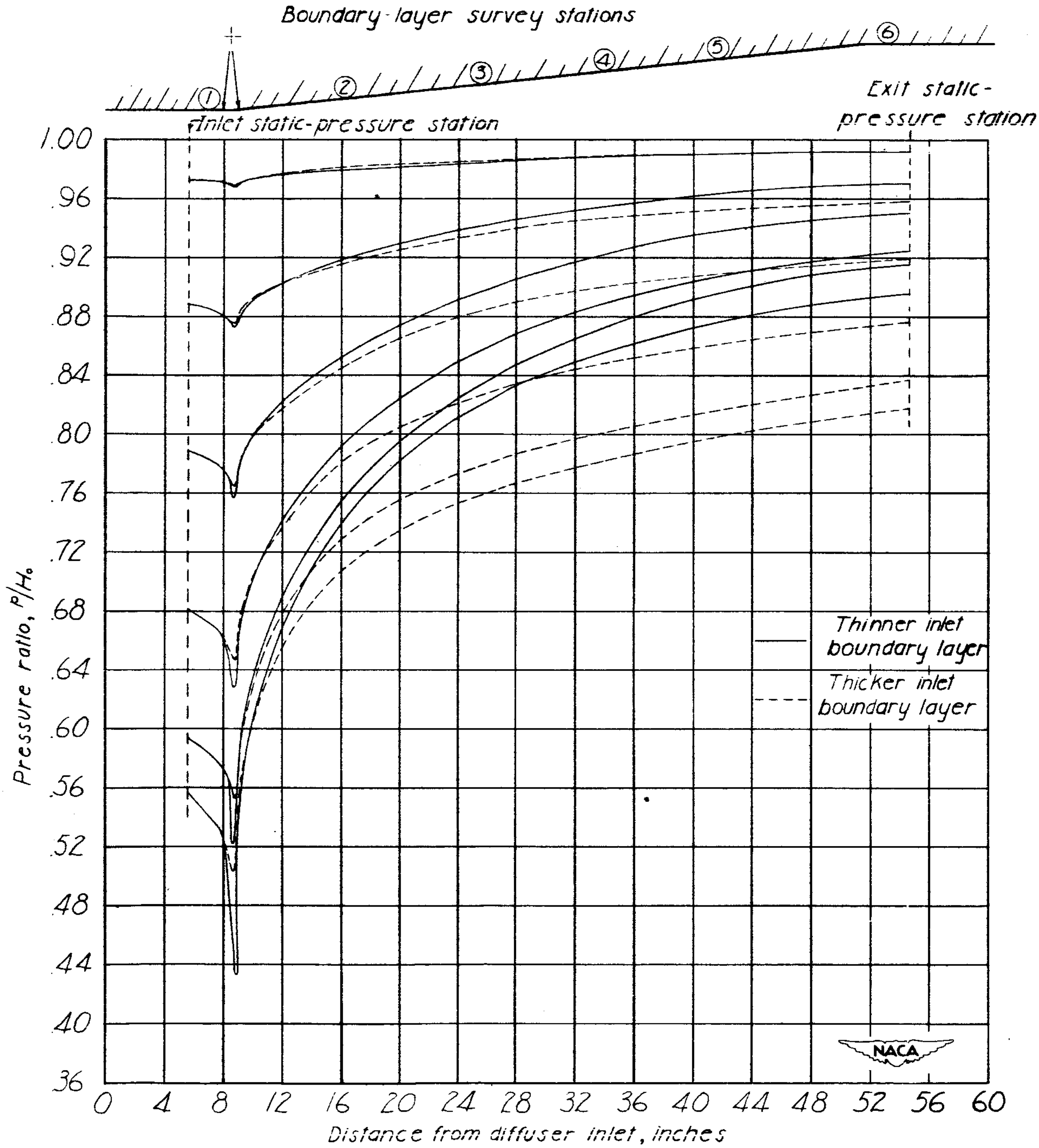

Figure 11.- Comparison of static-pressure distributions.

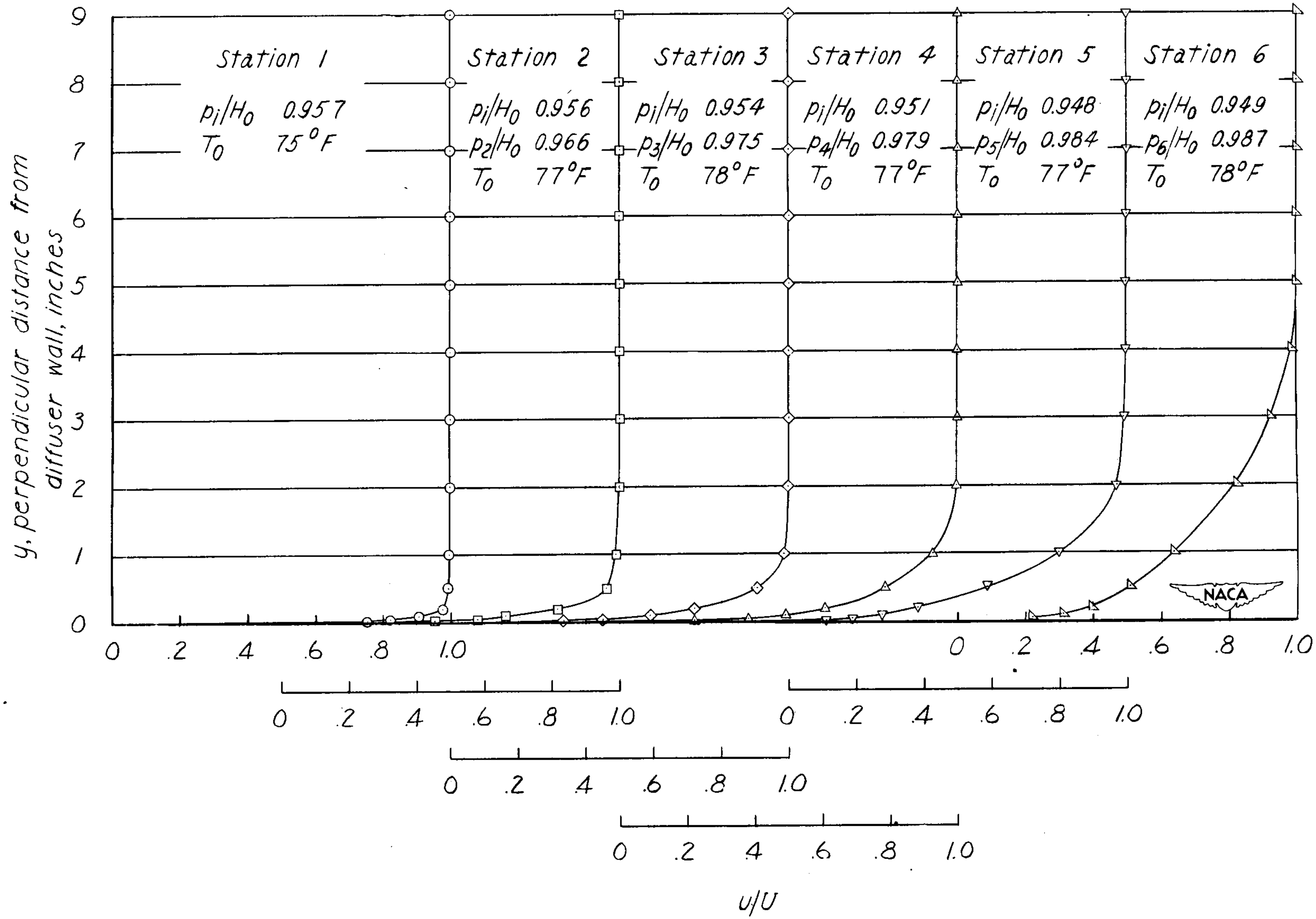

(a) $\frac{p_i}{H_0} \cong 0.95$.

Figure 12.- Boundary-layer growth in diffuser with thinner inlet boundary layer.

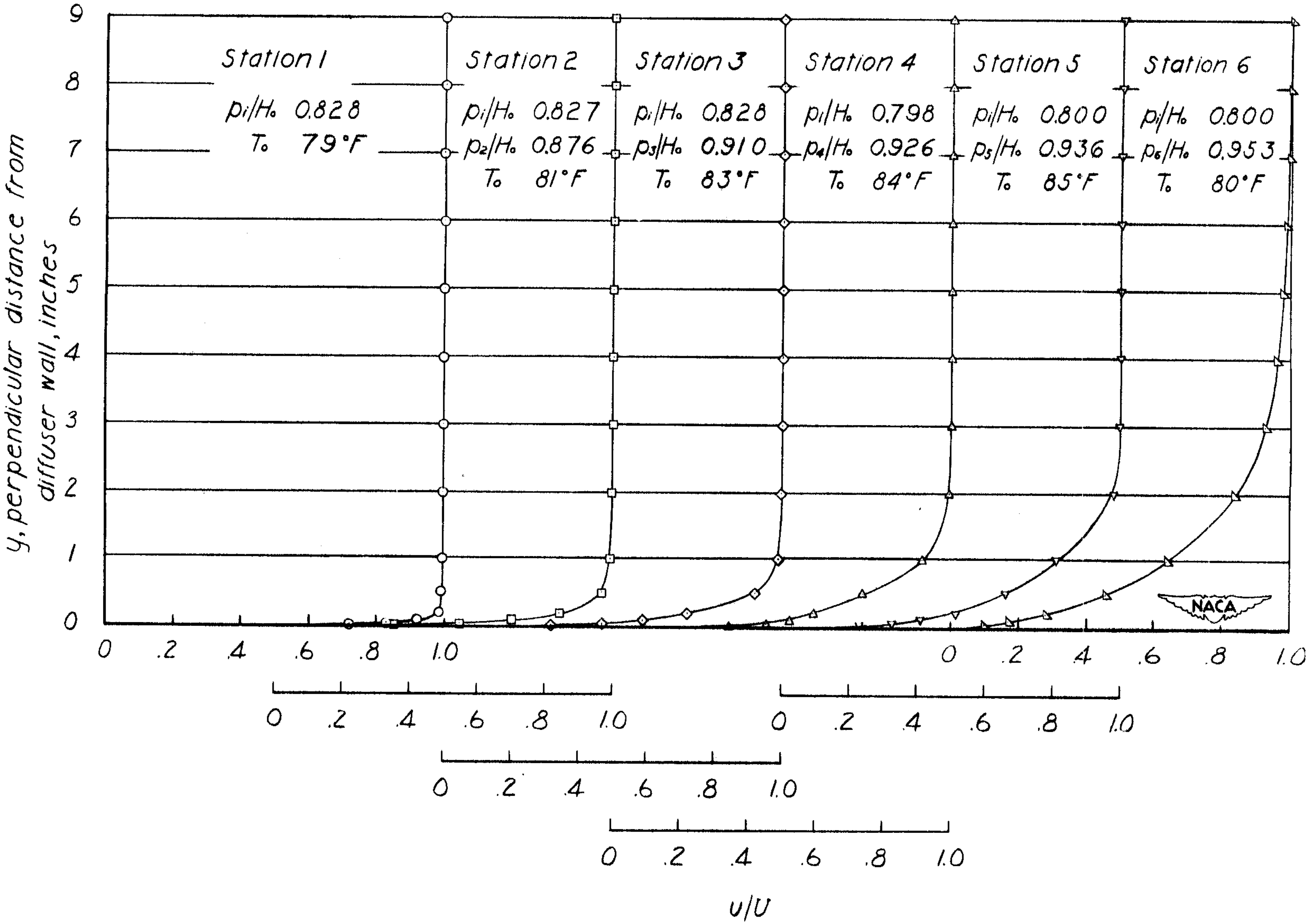

(b) $\frac{p_1}{H_o} \approx 0.80$.

Figure 12.- Continued.

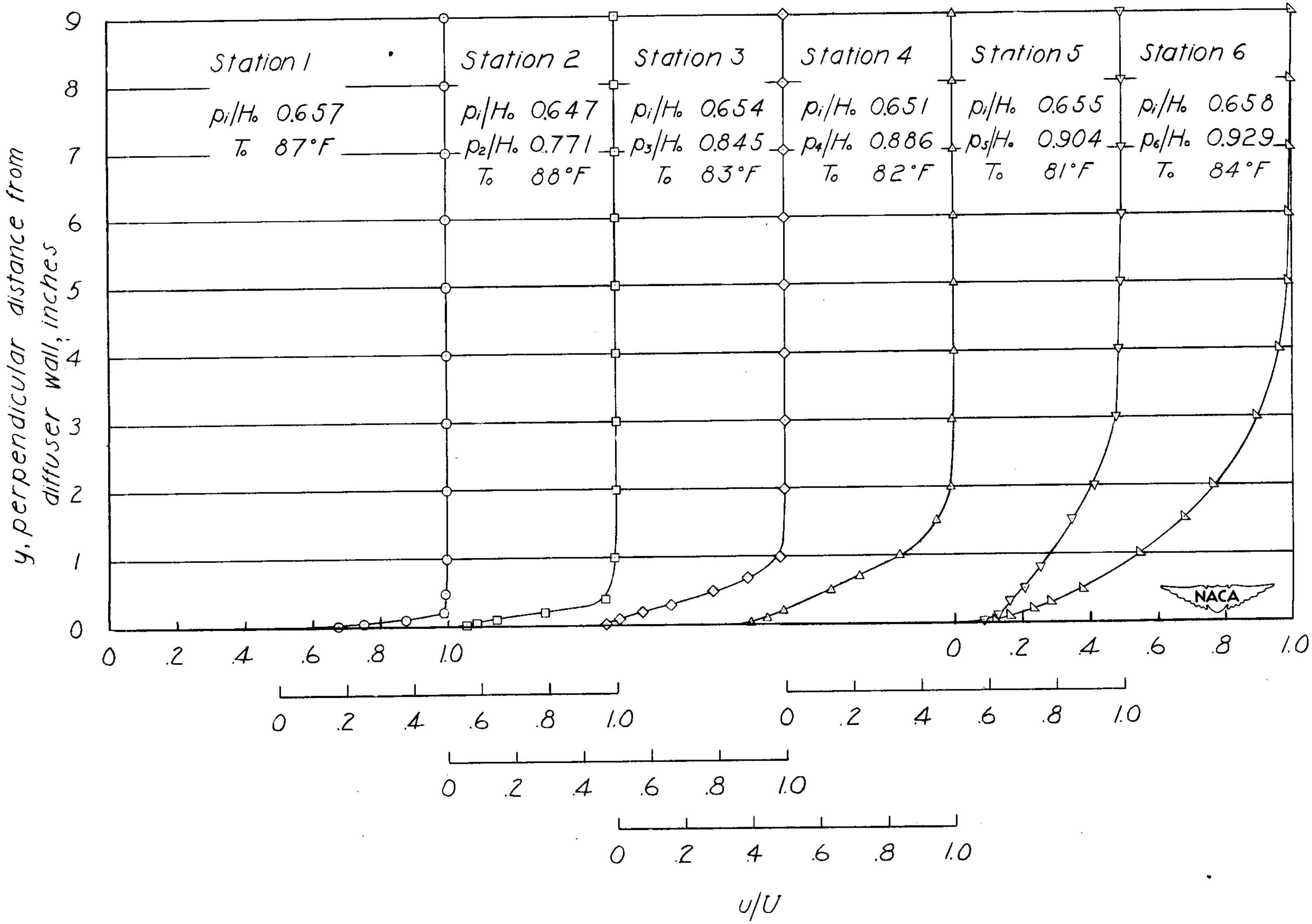

(c) $\frac{p_1}{H_0} \cong 0.65$.

Figure 12.- Continued.

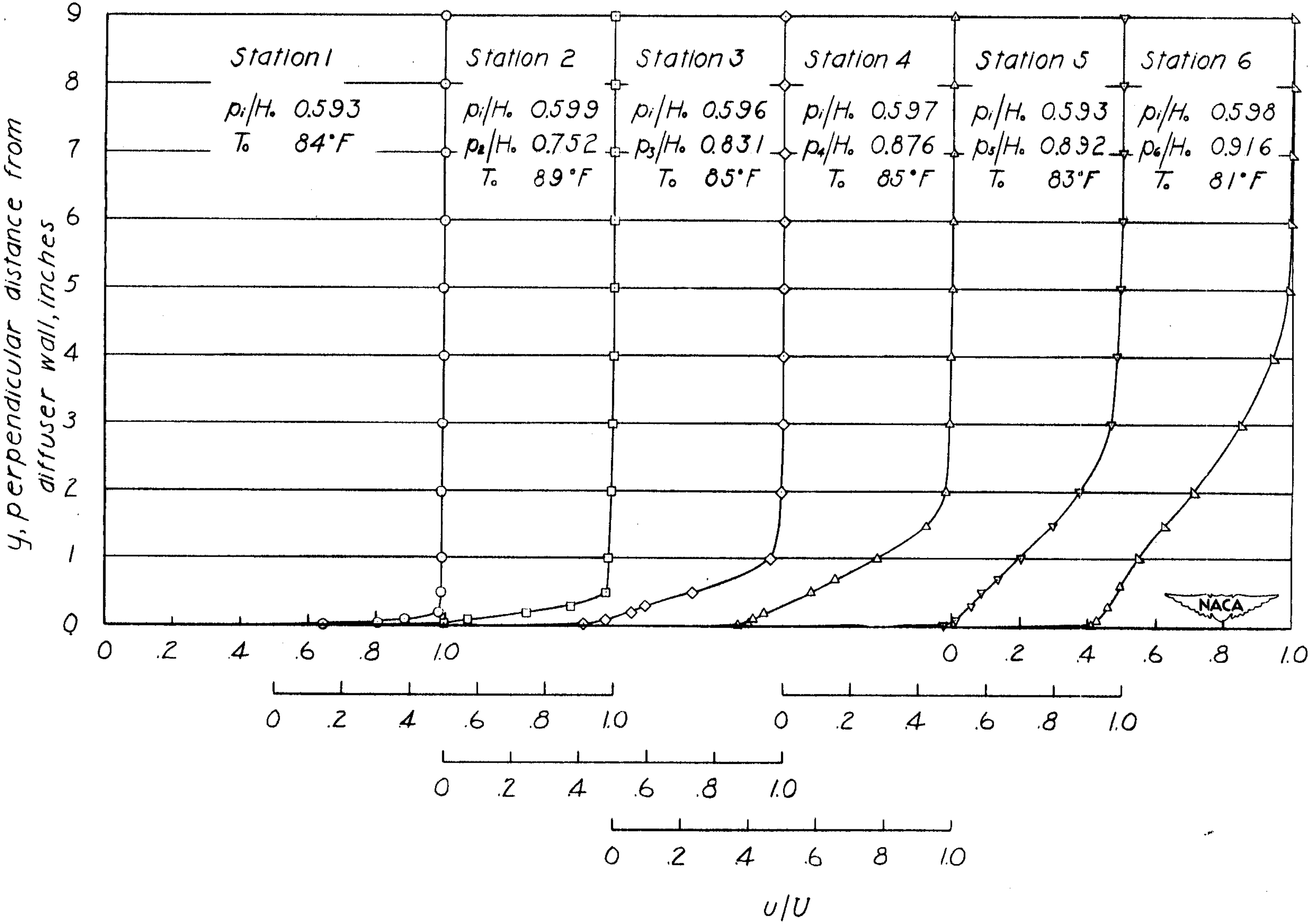

(d) $\frac{p_1}{H_0} \cong 0.59$.

Figure 12.- Continued.

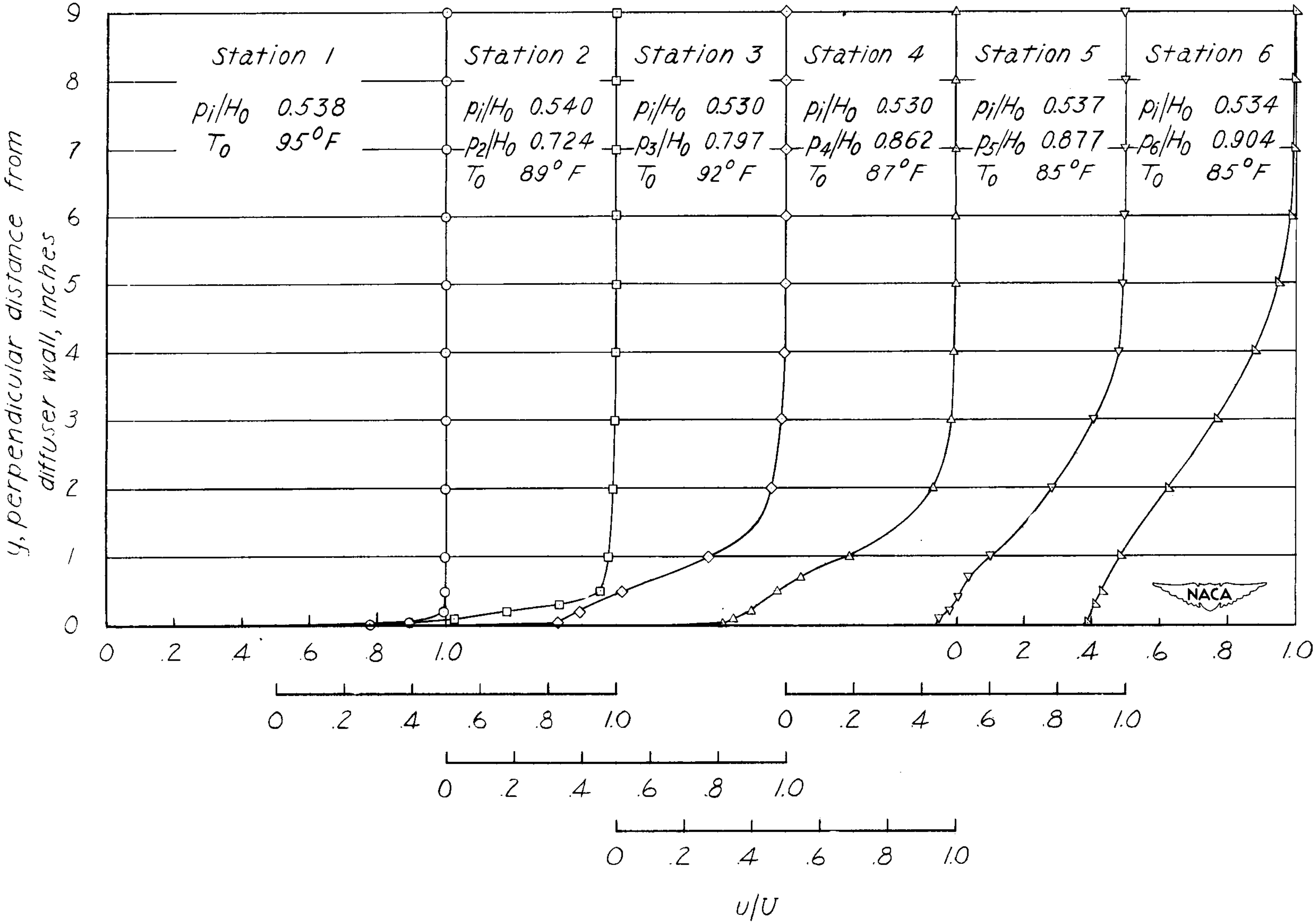

(e) $\frac{p_i}{H_0} \cong 0.53$.

Figure 12.- Concluded.

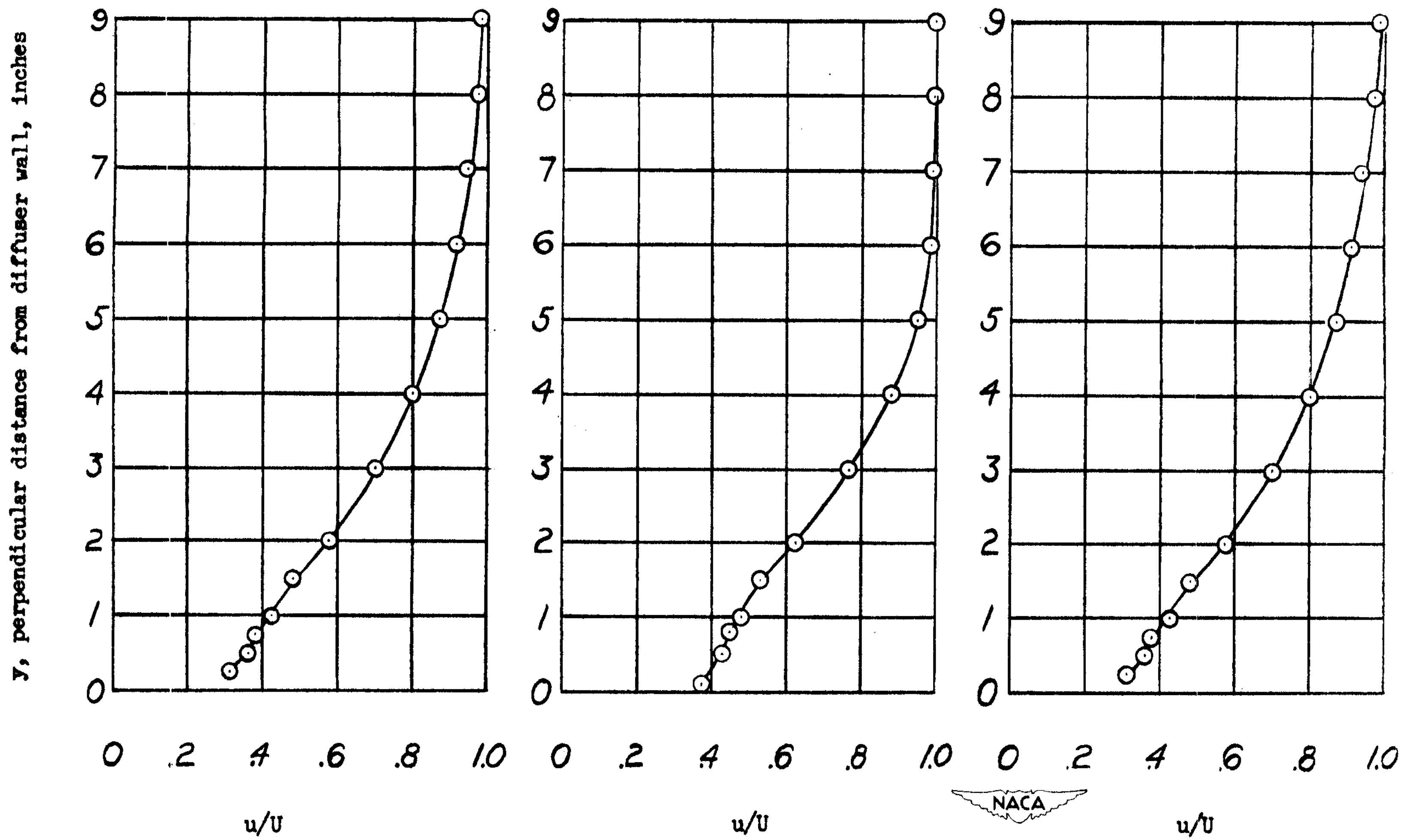

(a) $\frac{p_i}{H_o} = 0.542.$ (b) $\frac{p_i}{H_o} = 0.534.$ (c) $\frac{p_i}{H_o} = 0.542.$

Figure 13.- Boundary-layer profiles 120° apart on circumference of diffuser with thinner inlet boundary layer, station 6.

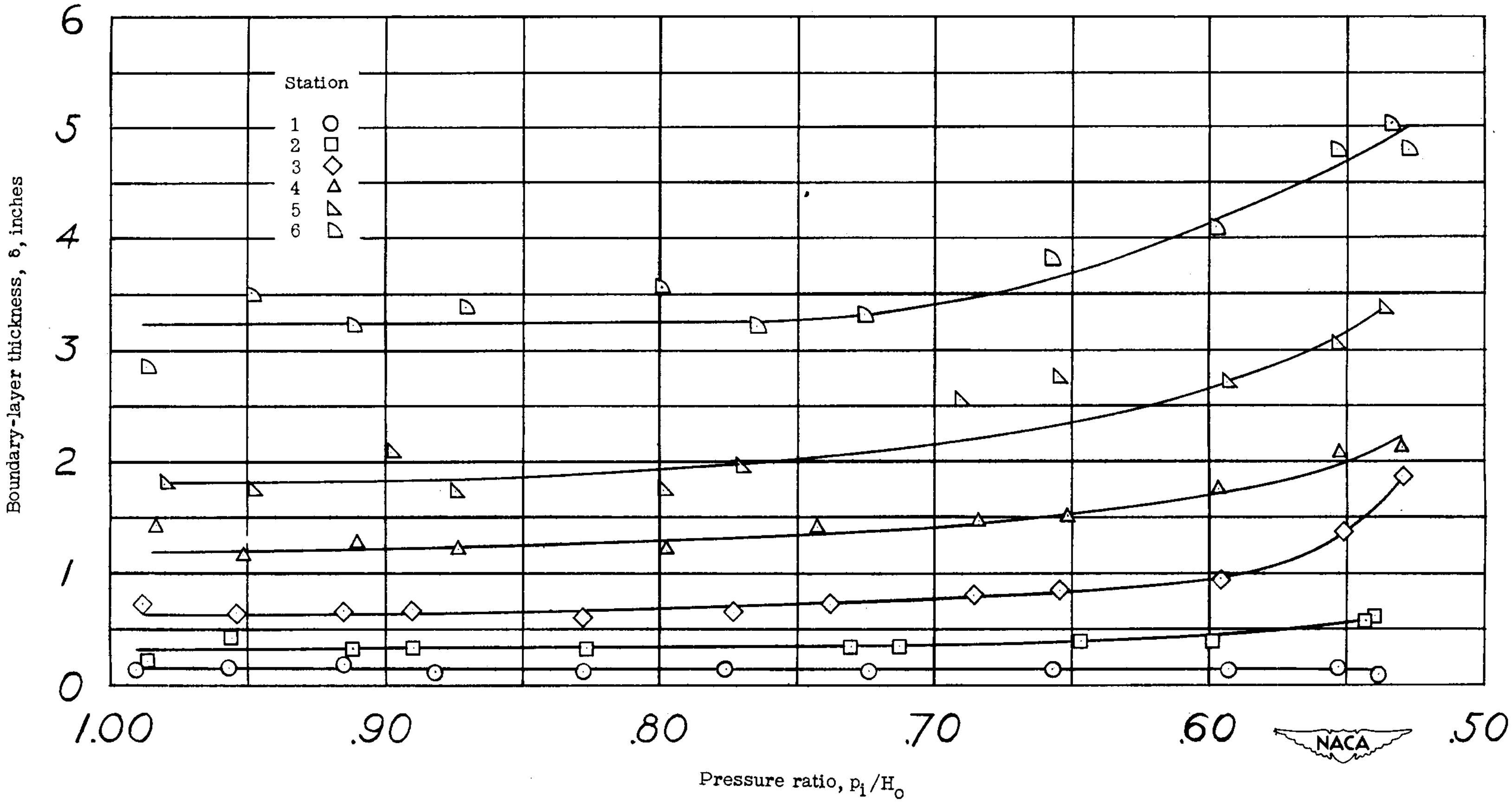

Figure 14.- Variation of boundary-layer thickness with pressure ratio, thinner inlet boundary layer.

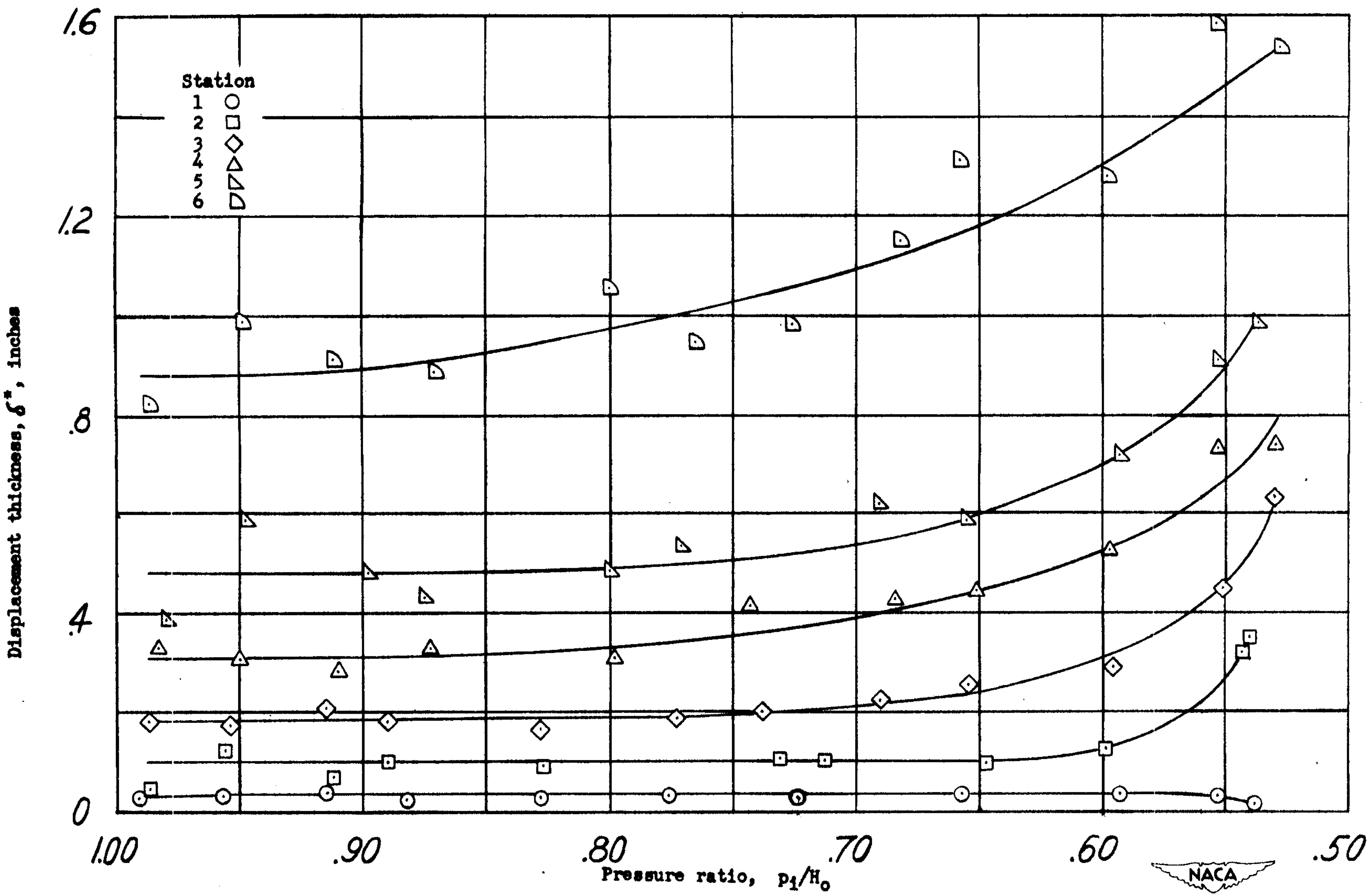

Figure 15.- Variation of displacement thickness with pressure ratio, thinner inlet boundary layer.

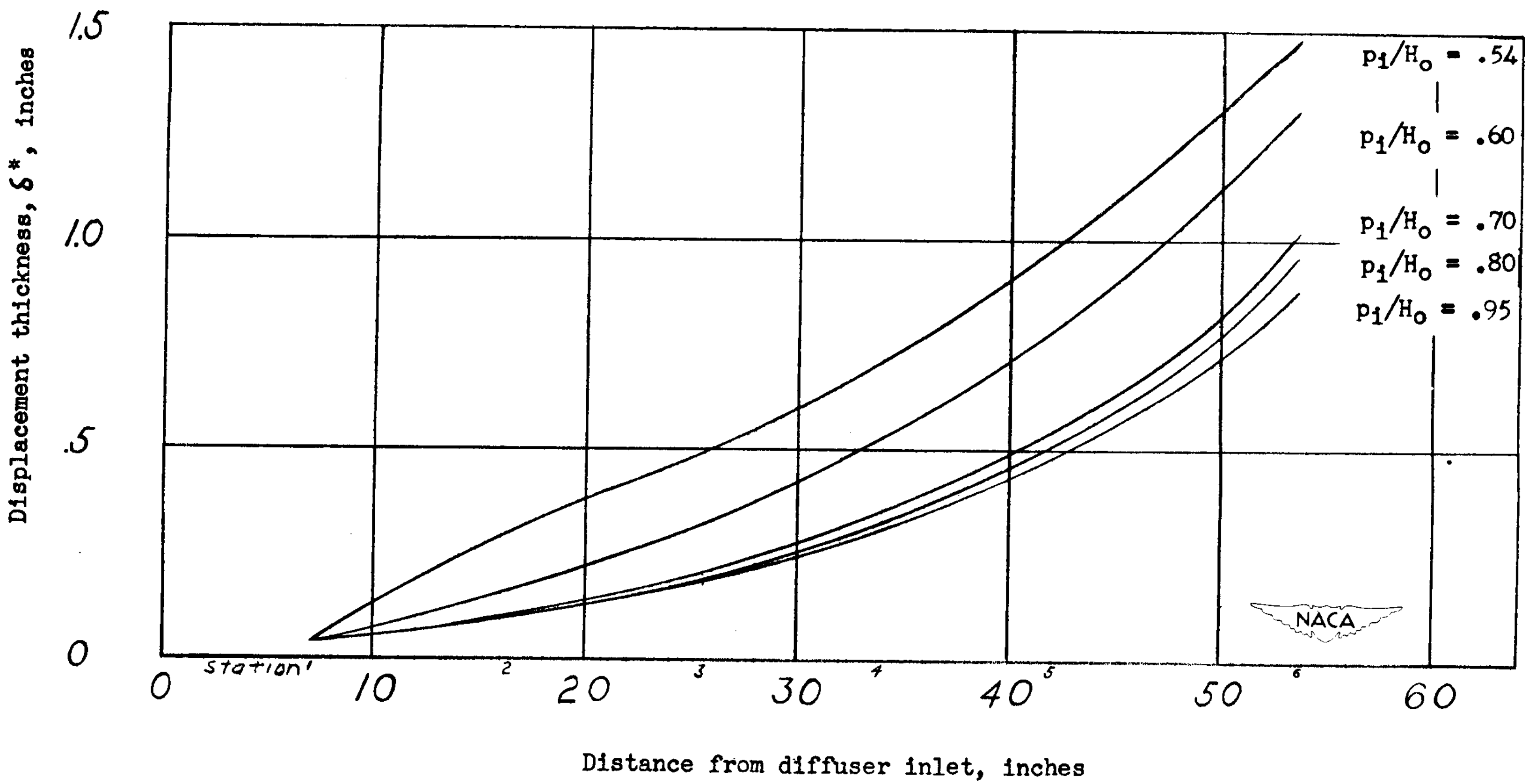

Figure 16.- Growth of displacement thickness in thinner-inlet-boundary-layer diffuser.

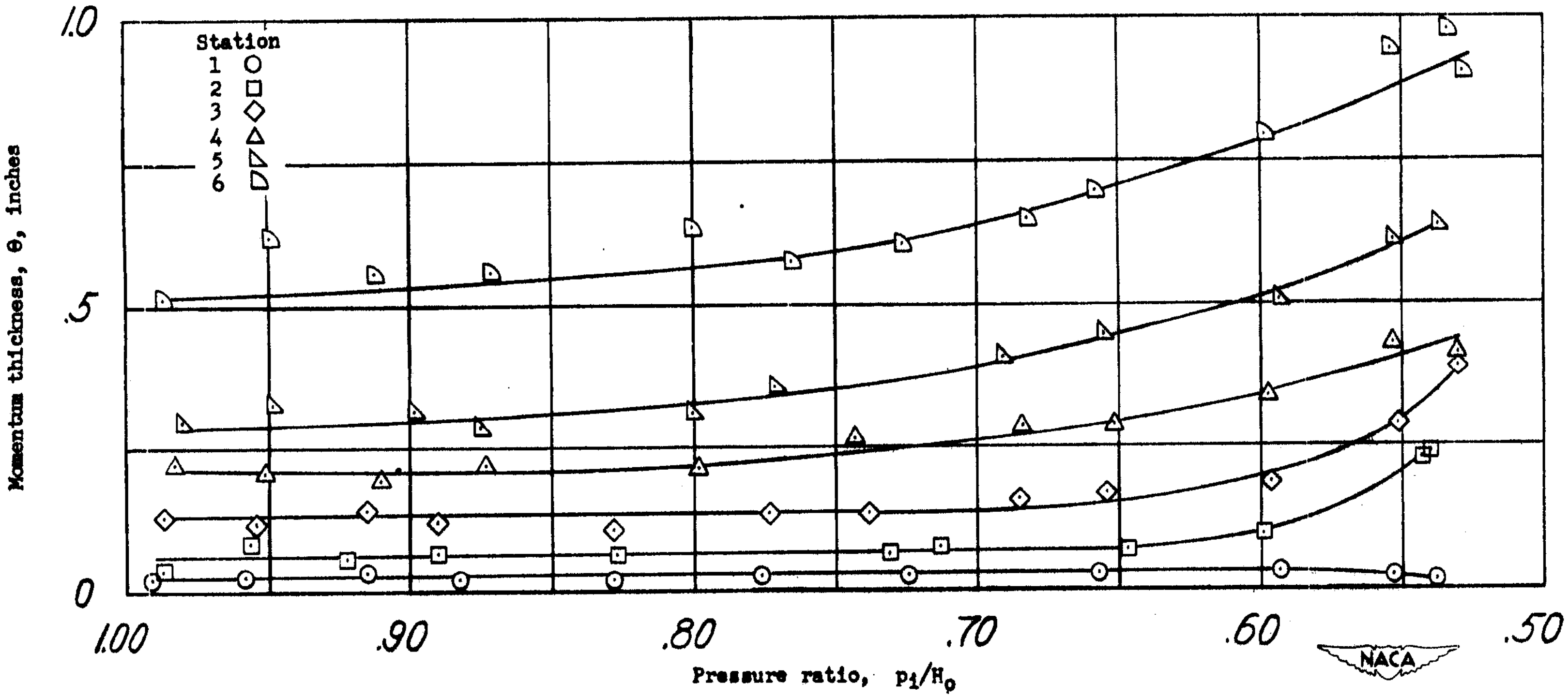

Figure 17.- Variation of momentum thickness with pressure ratio, thinner inlet boundary layer.

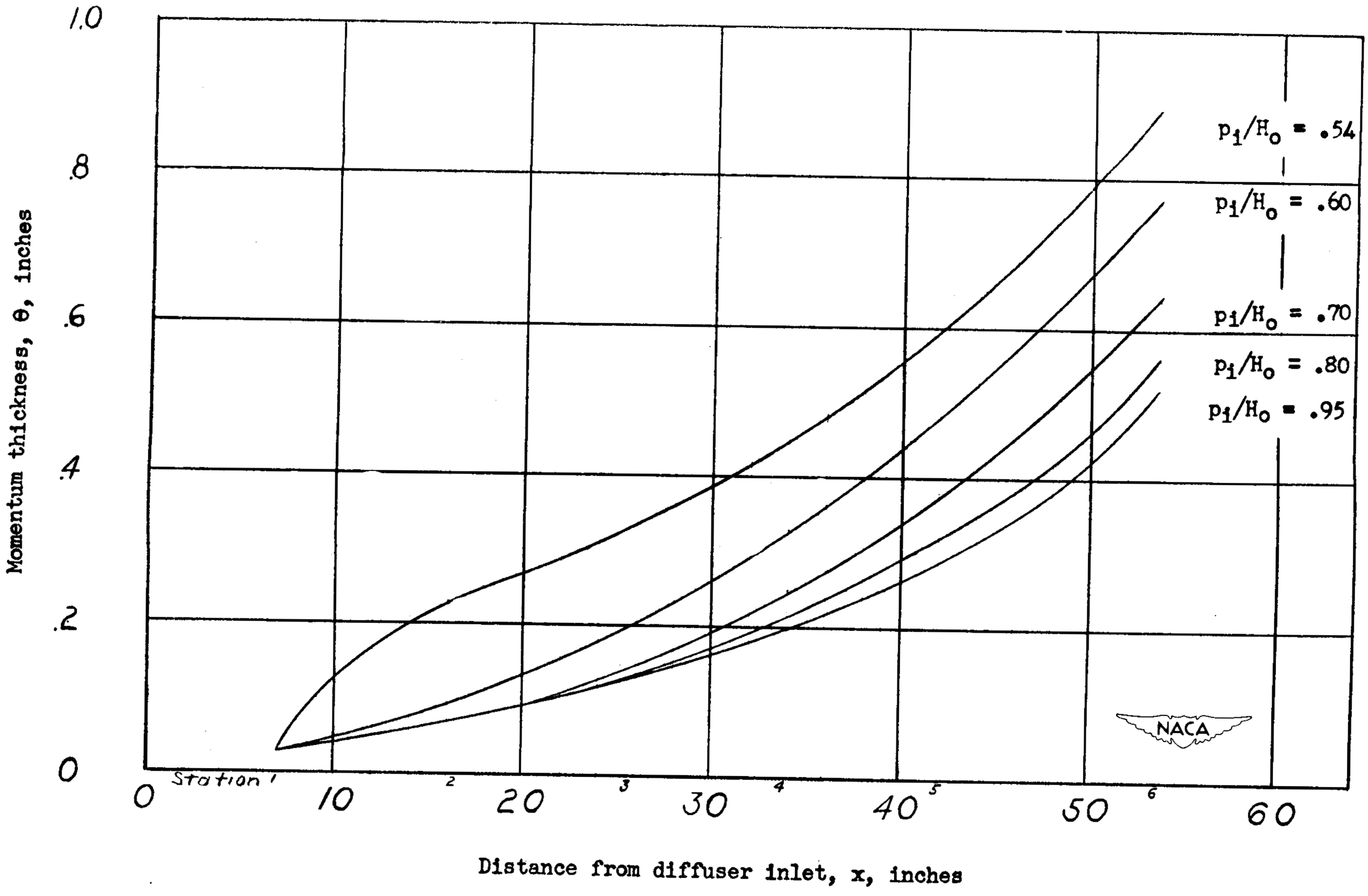

Figure 18.- Growth of momentum thickness in thinner-inlet-boundary-layer diffuser.

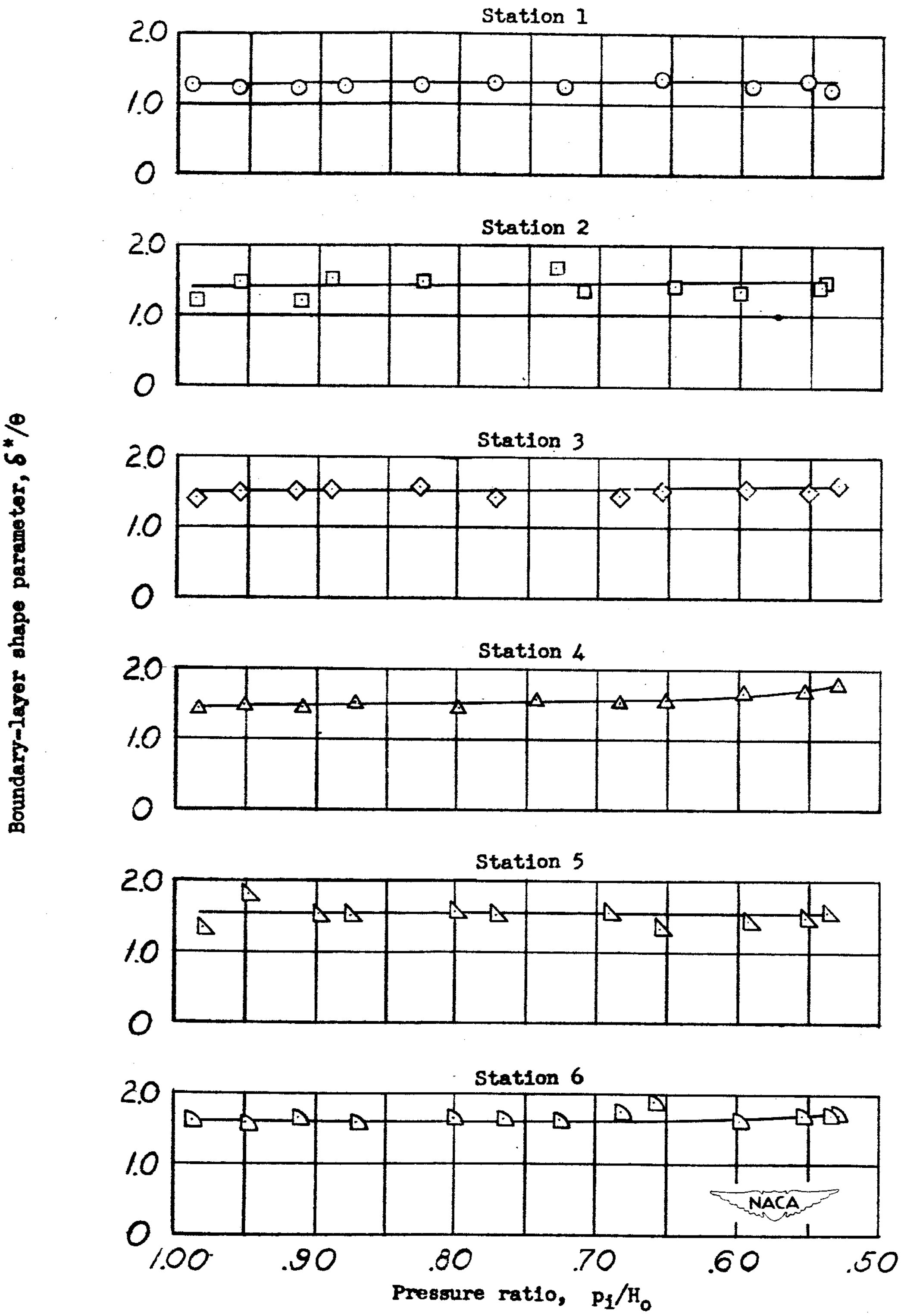

Figure 19.- Variation of boundary-layer shape parameter with pressure ratio, thinner inlet boundary layer.

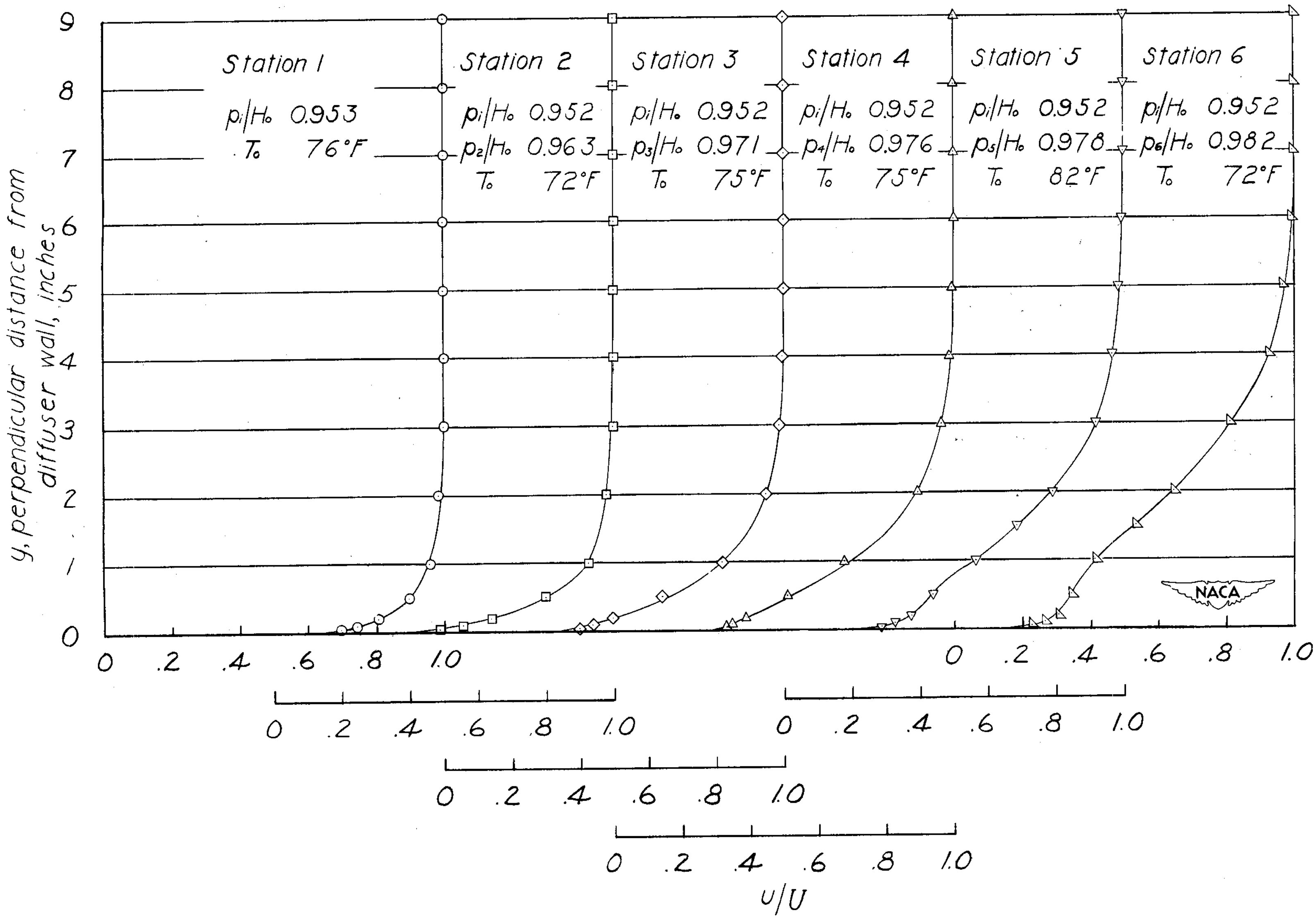

(a) $\frac{p_i}{H_0} \cong 0.95$.

Figure 20.- Boundary-layer growth in diffuser with thicker inlet boundary layer.

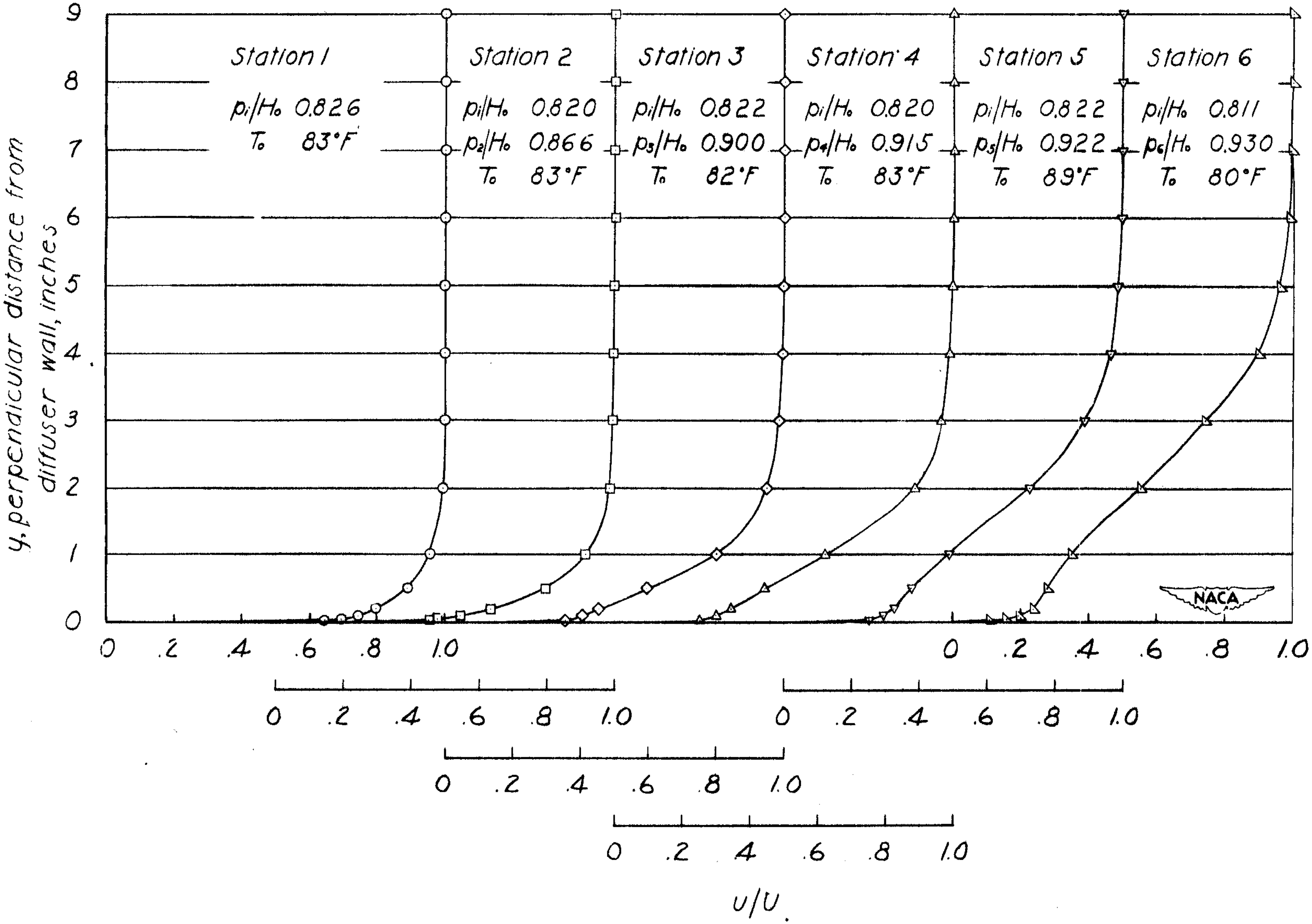

(b) $\frac{p_1}{H_0} \cong 0.82$.

Figure 20.- Continued.

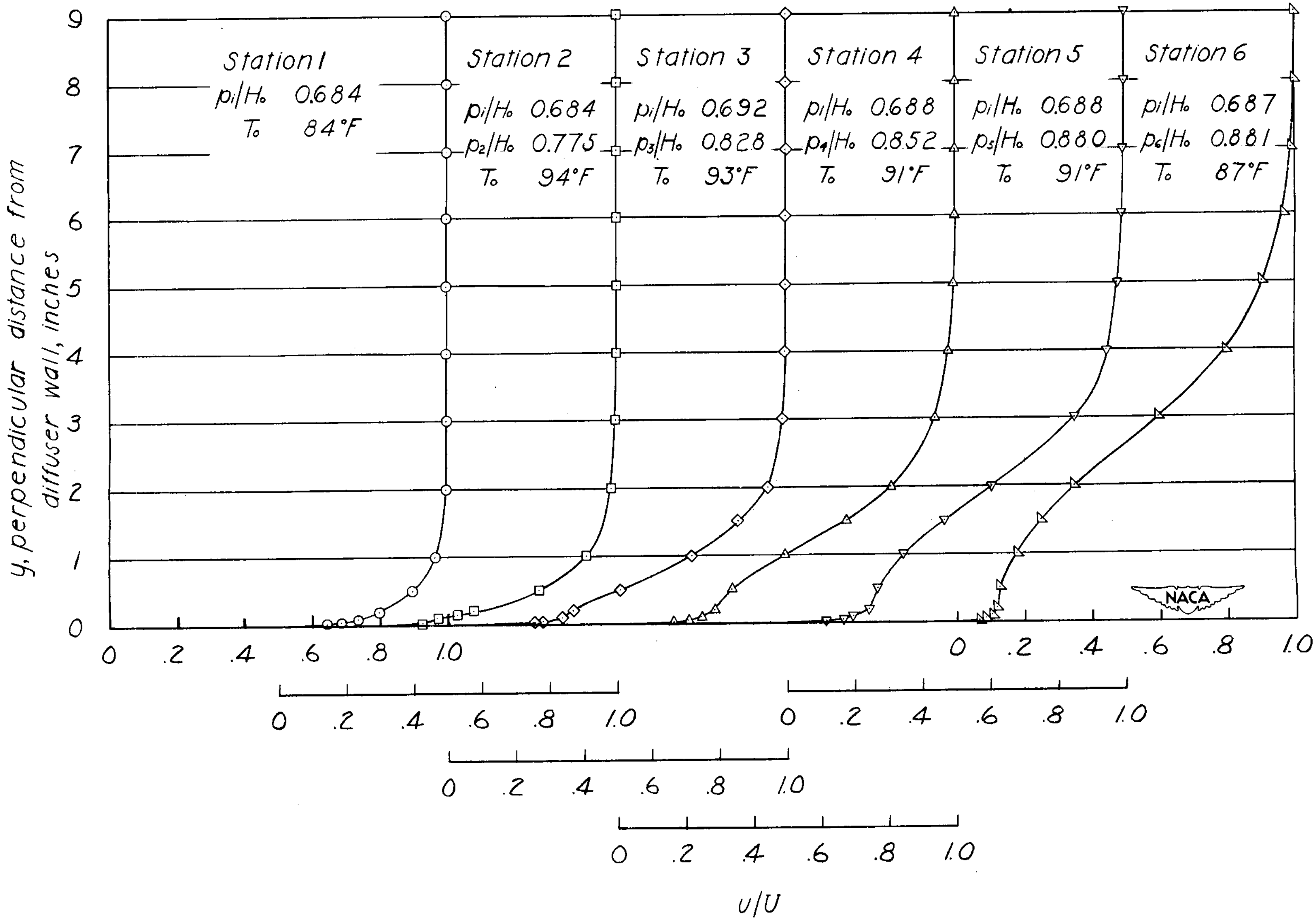

(c) $\frac{p_1}{H_0} \cong 0.68$.

Figure 20.- Continued.

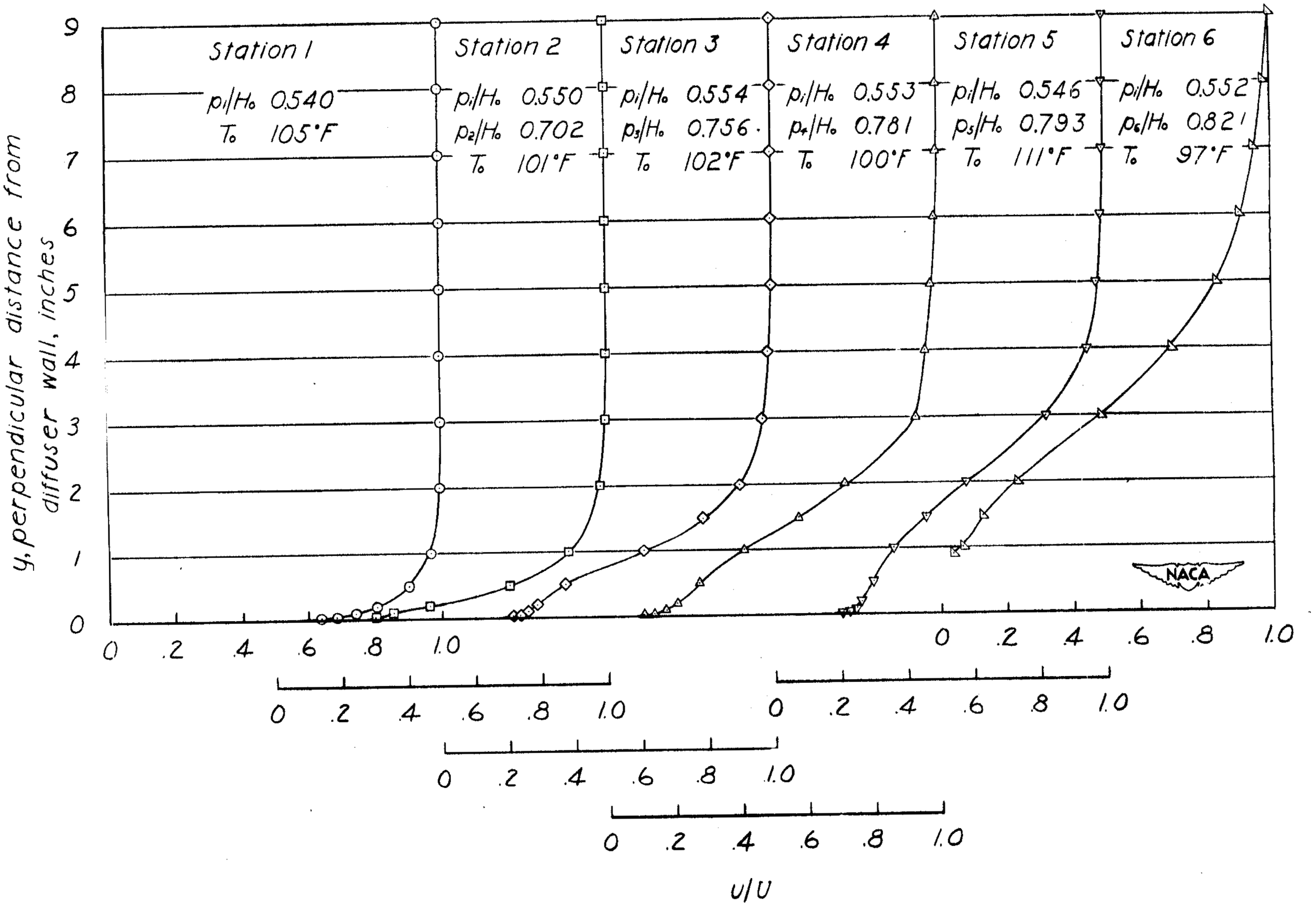

(d) $\frac{p_1}{H_o} \cong 0.55$.

Figure 20.- Continued.

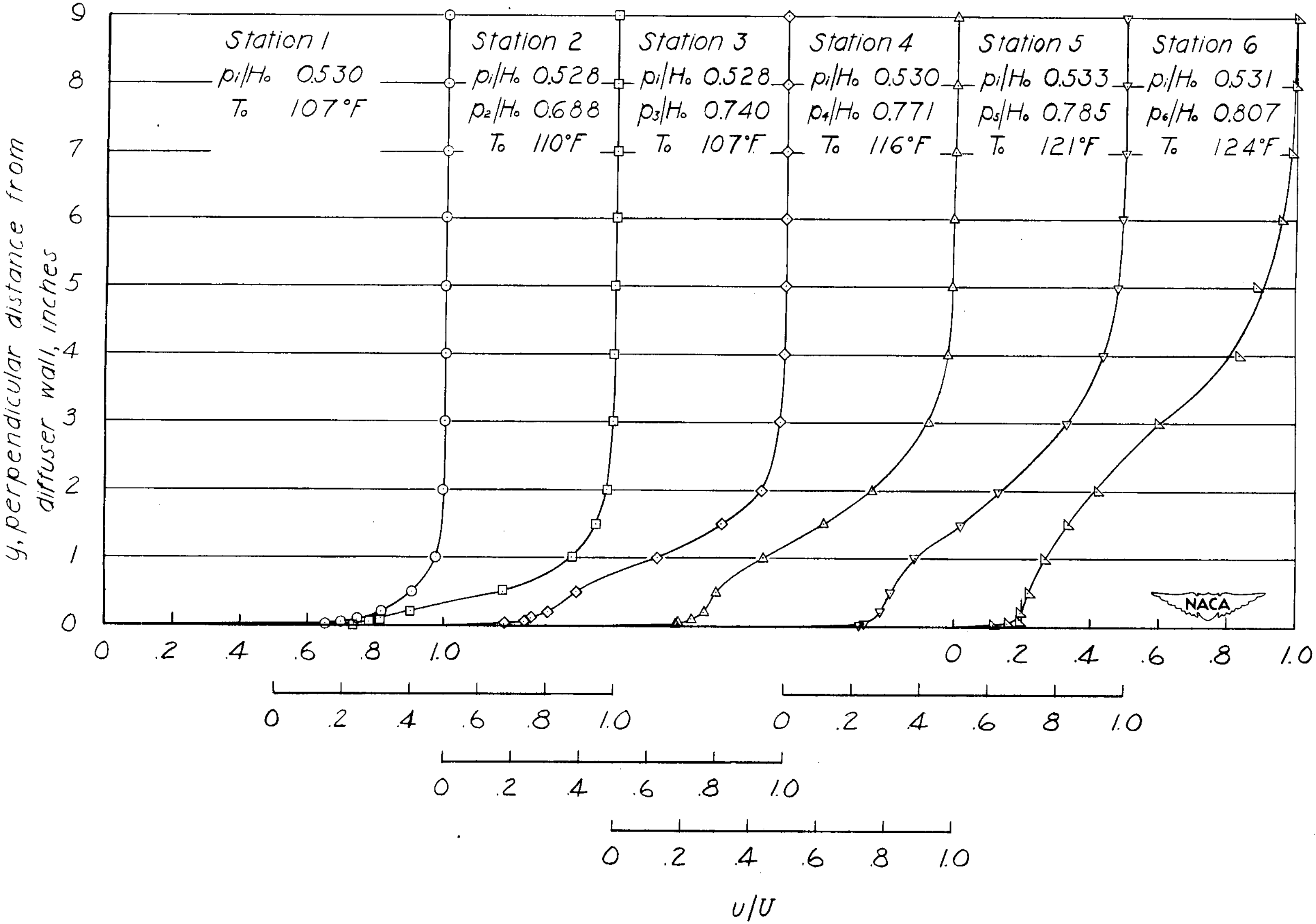

(e) $\frac{p_1}{H_o} \cong 0.53$.

Figure 20.- Concluded.

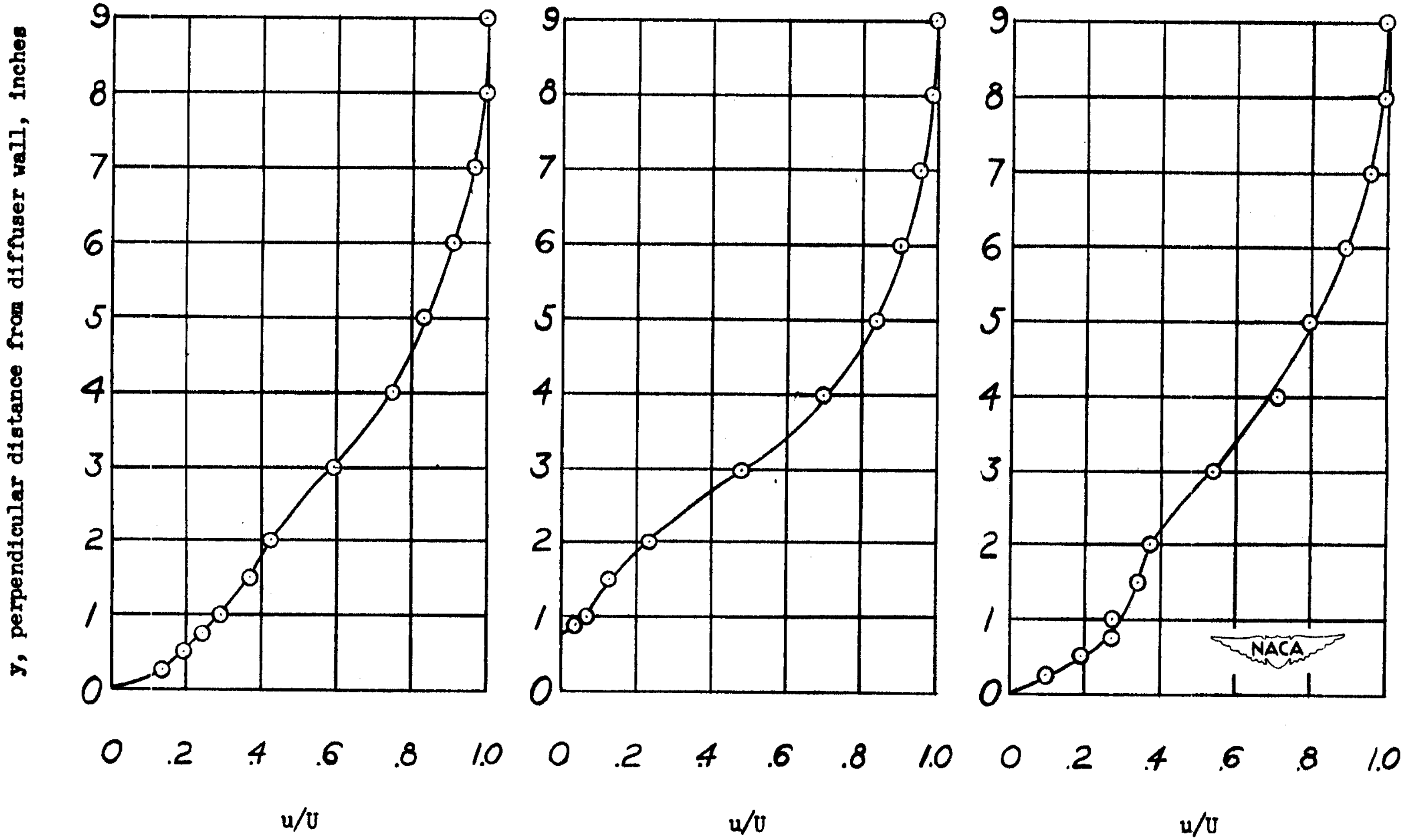

(a) $\frac{p_i}{H_o} = 0.551$. (b) $\frac{p_i}{H_o} = 0.552$. (c) $\frac{p_i}{H_o} = 0.551$.

Figure 21.- Boundary-layer profiles 120° apart on circumference of diffuser with thicker inlet boundary layer, station 6.

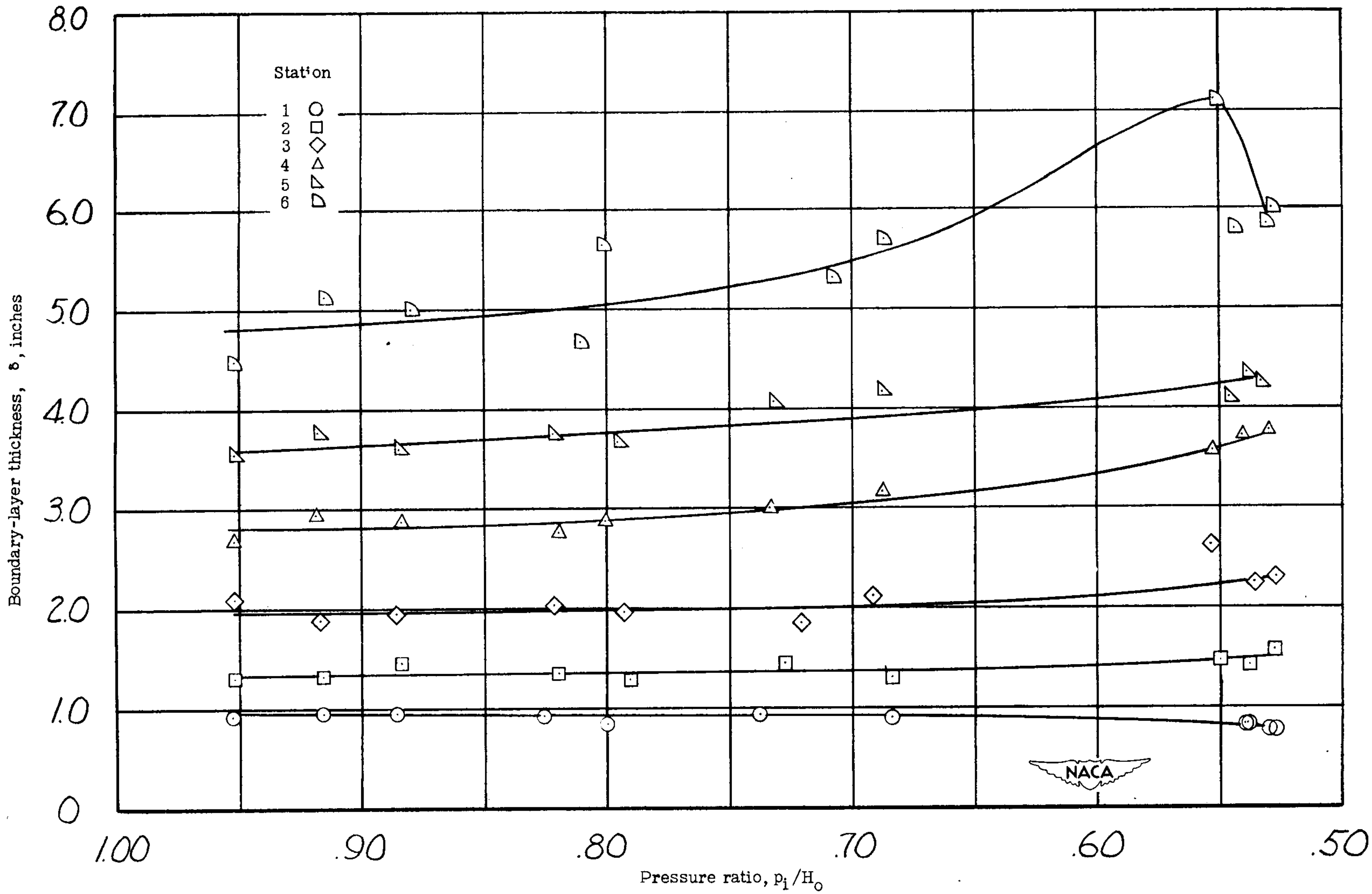

Figure 22.- Variation of boundary-layer thickness with pressure ratio, thicker inlet boundary layer.

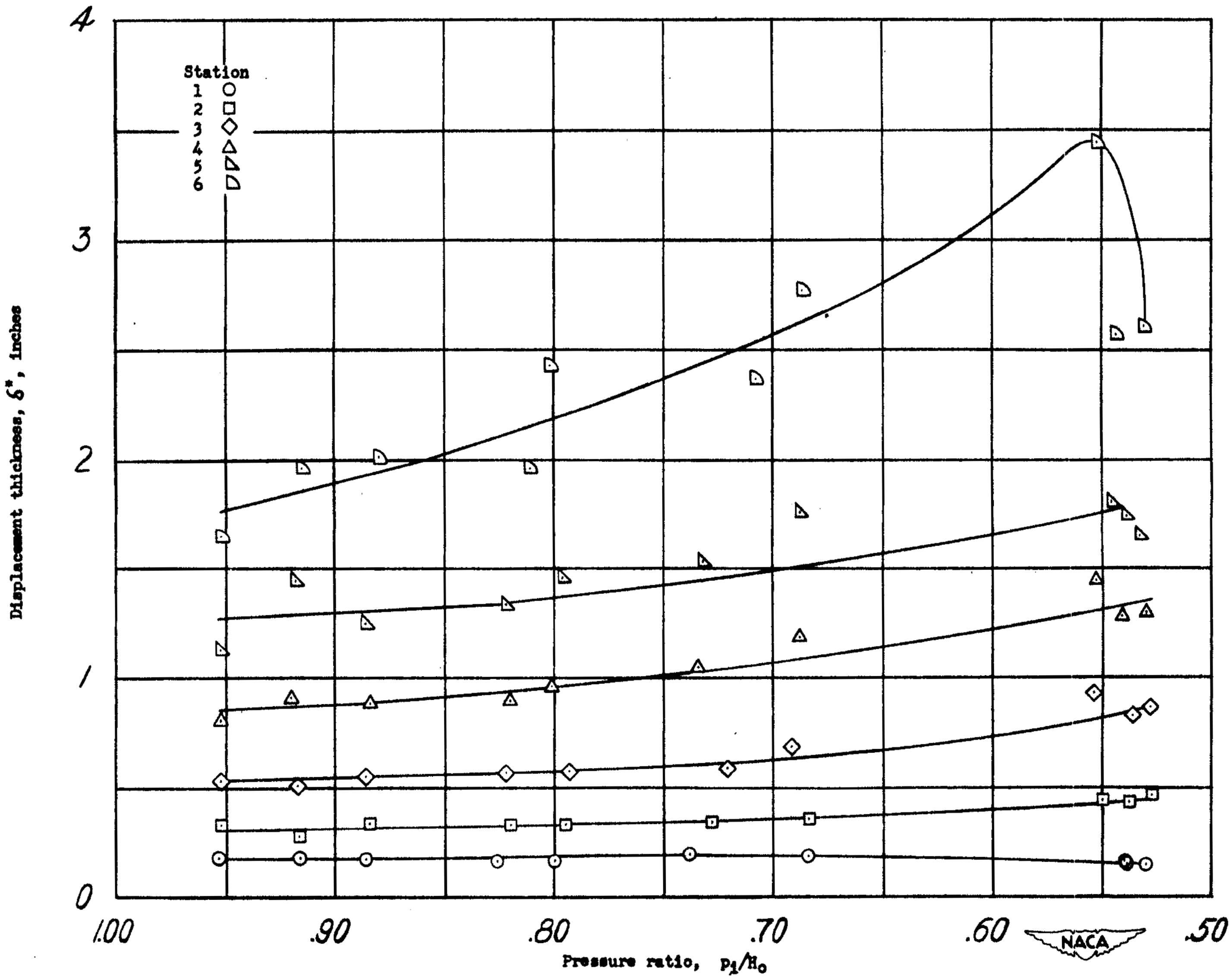

Figure 23.- Variation of displacement thickness with pressure ratio, thicker inlet boundary layer.

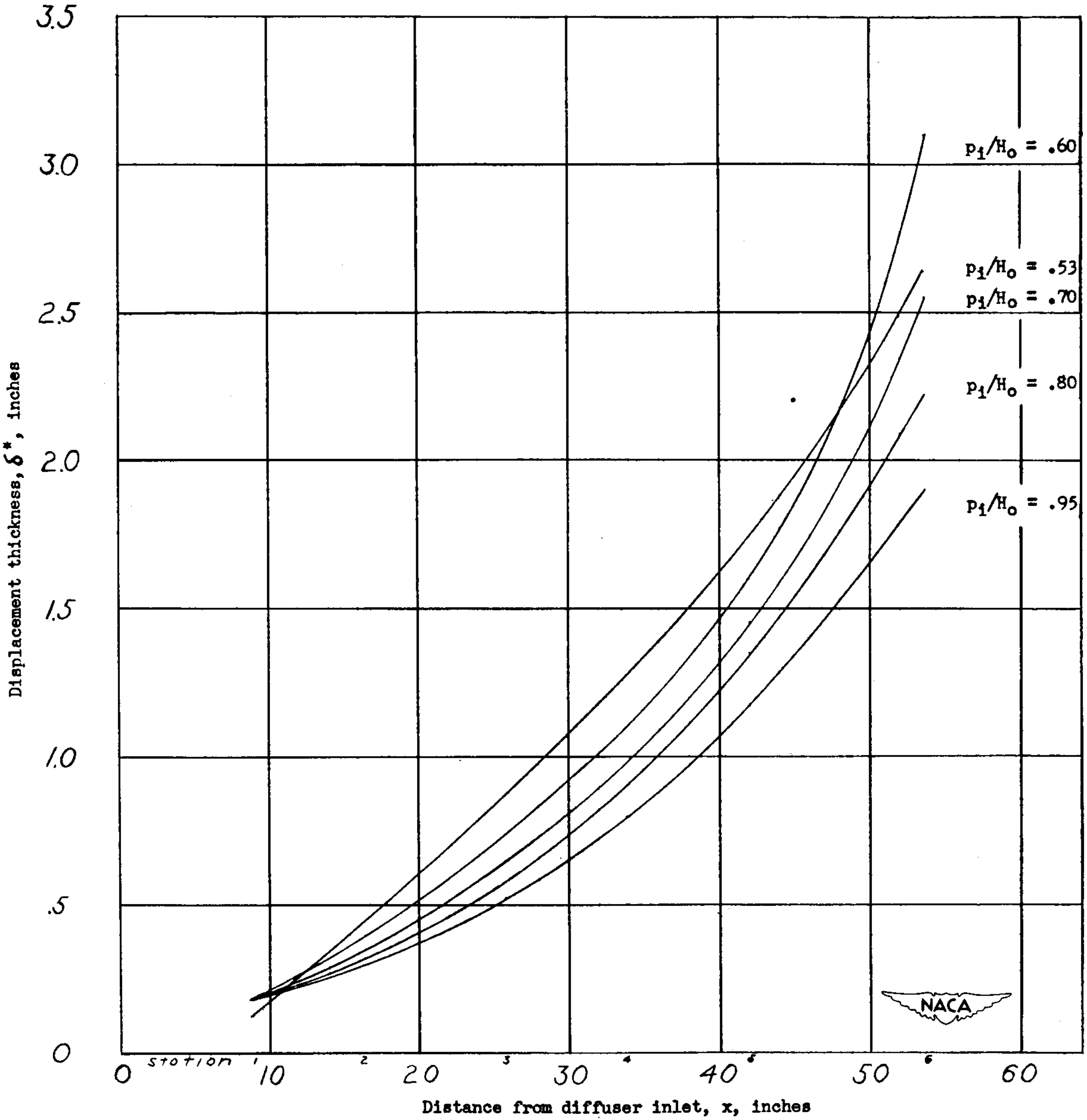

Figure 24.- Growth of displacement thickness in thicker-inlet-boundary-layer diffuser.

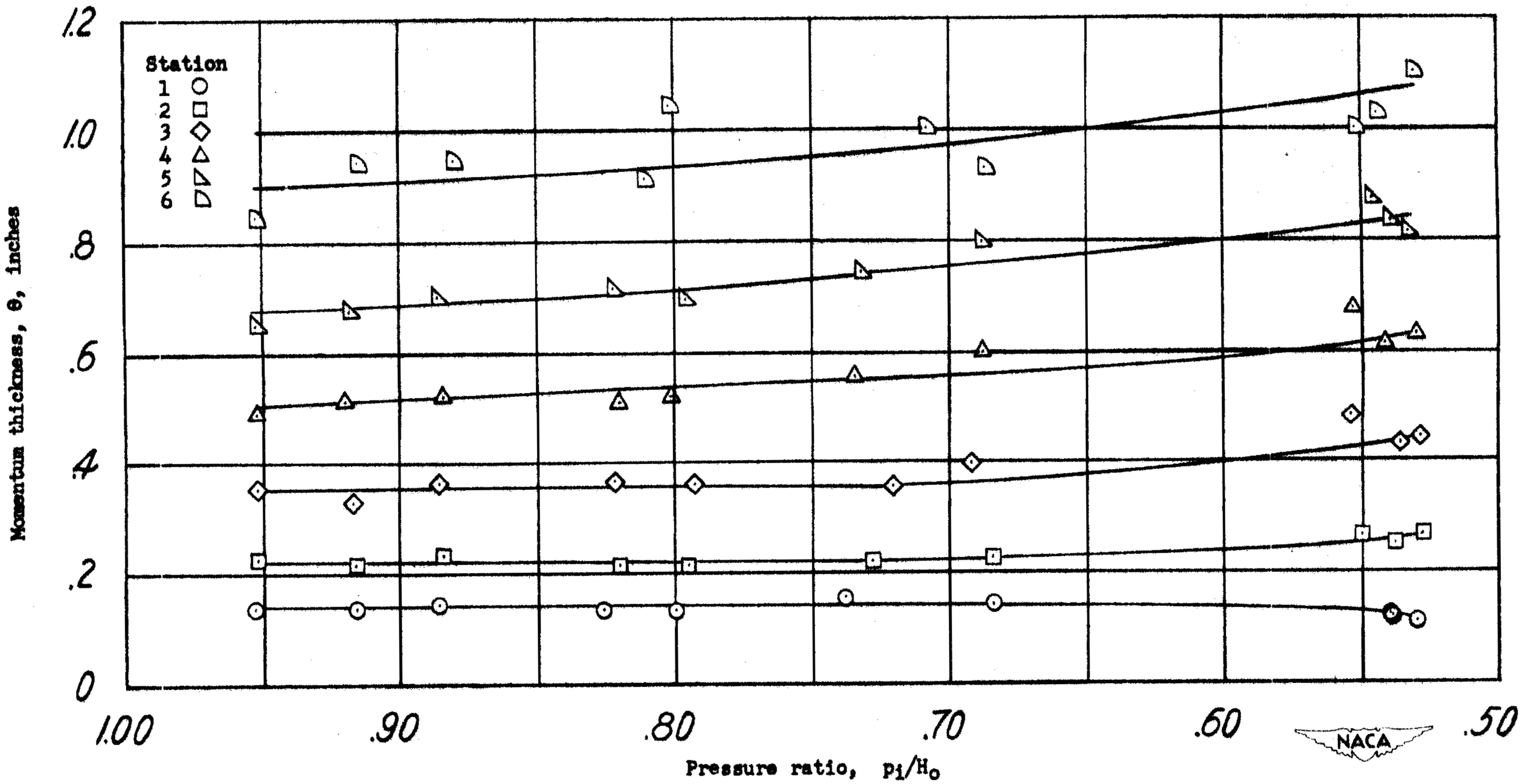

Figure 25.- Variation of momentum thickness with pressure ratio, thicker inlet boundary layer.

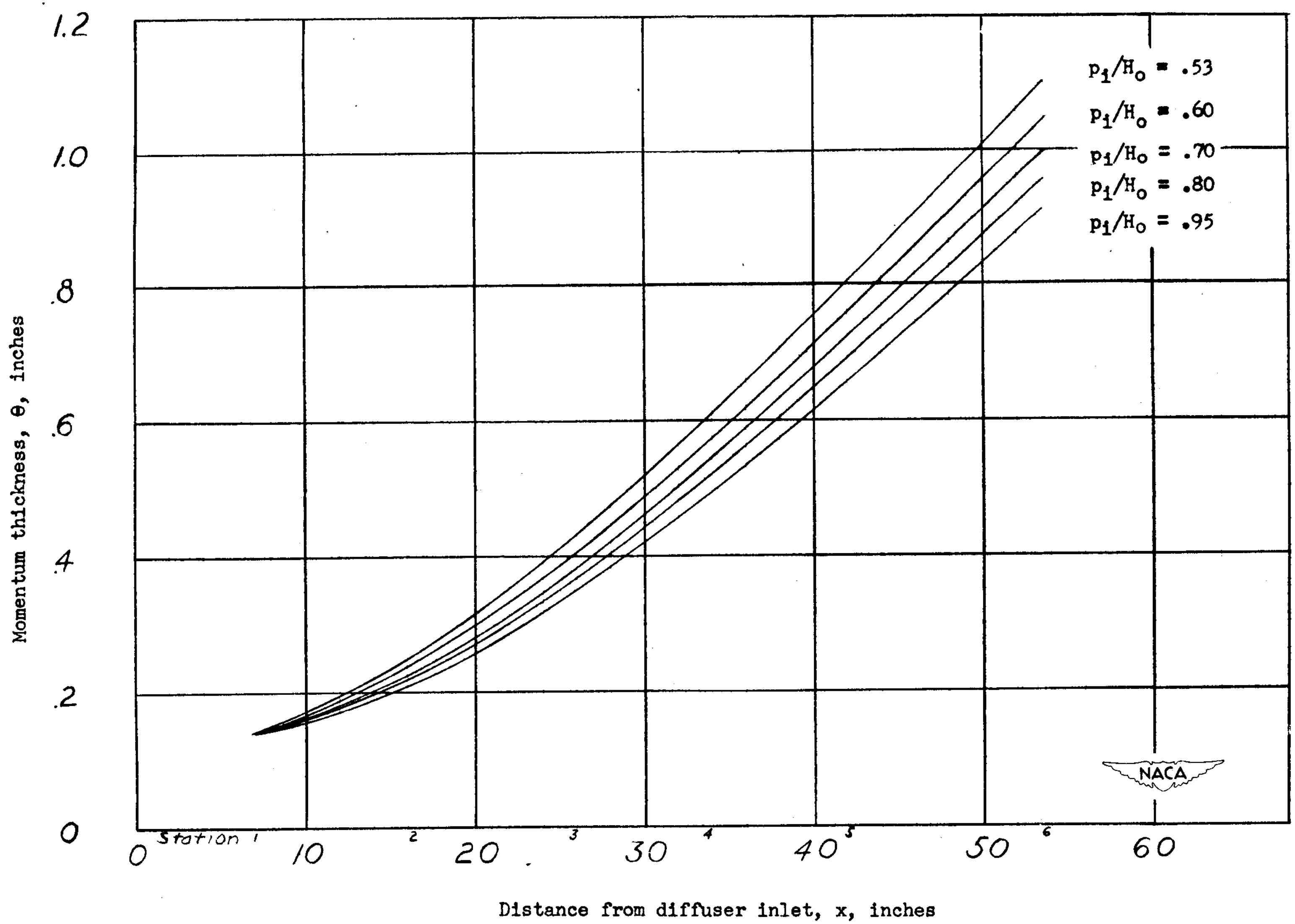

Figure 26.- Growth of momentum thickness in thicker-inlet-boundary-layer diffuser.

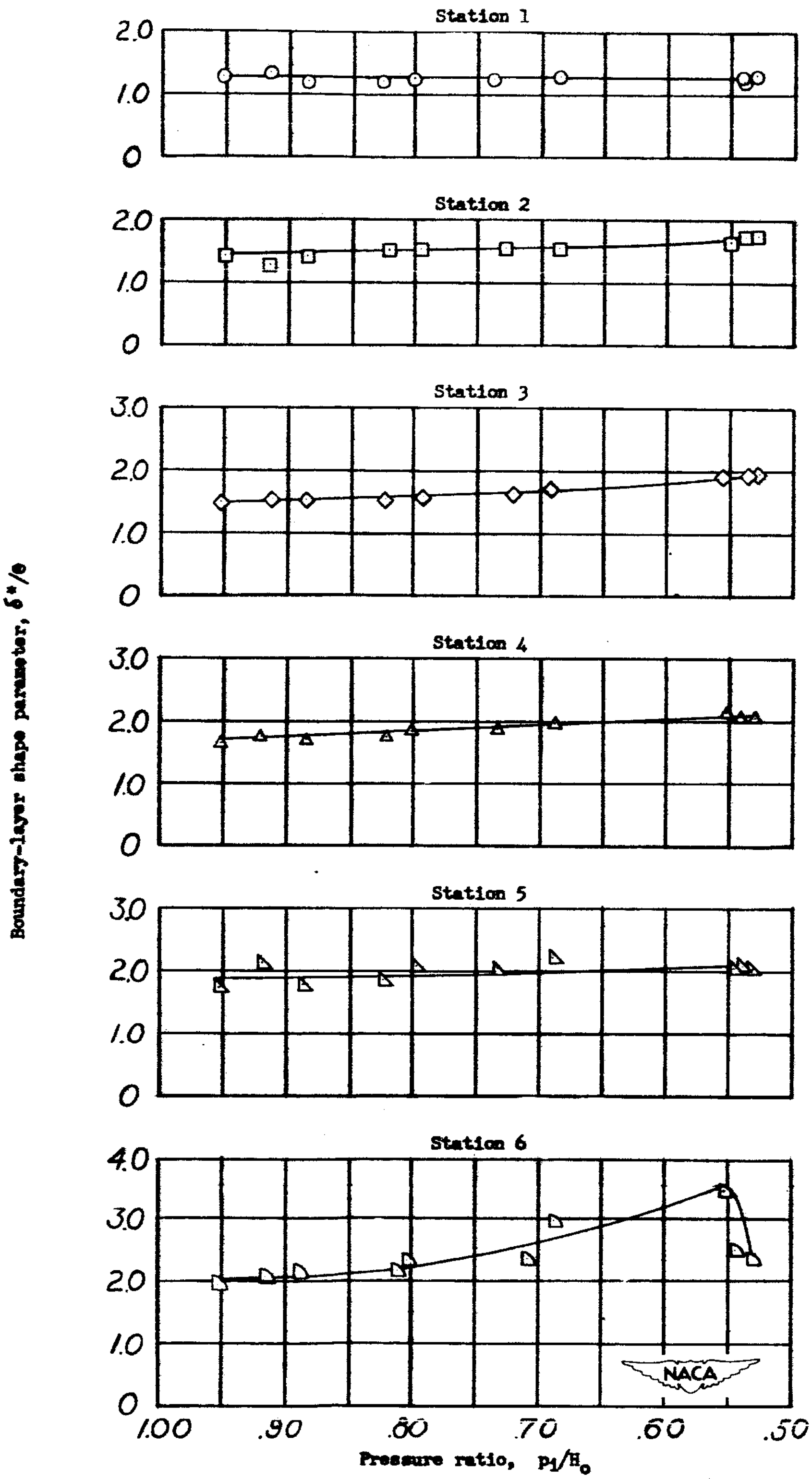

Figure 27.- Variation of boundary-layer shape parameter with pressure ratio, thicker inlet boundary layer.